land

MDPI

Article

Assessing the Impacts of Urbanization and Climate Change on NPP Under Different Habitat Quality Conditions over the Last Two Decades in the Tibetan Plateau, China

Tanlong Xia [1,†], Liusheng Han [1,†], Chen Ren [1], Qian Xu [1], Dafu Zhang [1], Guangwei Sun [1] and Zhaohui Feng [2,*]

[1] School of Civil Engineering and Geomatics, Shandong University of Technology, Zibo 255000, China; 23507020857@stumail.sdut.edu.cn (T.X.); hanls@sdut.edu.cn (L.H.); 23507020858@stumail.sdut.edu.cn (C.R.); 24507020872@stumail.sdut.edu.cn (Q.X.); zbzdf@sdut.edu.cn (D.Z.); sun100711@sdut.edu.cn (G.S.)

[2] College of Urban and Environmental Sciences, Peking University, Beijing 100871, China

* Correspondence: fengzh@igsnrr.ac.cn

† These authors contributed equally to this work.

Abstract: The processes of urbanization and climate change have exerted a marked influence on net primary productivity (NPP). However, the underlying mechanisms that drive these effects remain intricate and insufficiently understood. The processes of urbanization and climate change both have an adverse effect on habitat quality (HQ) and biodiversity loss. The HQ has a direct influence on the health and stability of ecosystems, which regulate the level of NPP. A higher HQ is associated with stronger NPP. Now, the quantification and assessment of the impacts of climate change and urbanization on NPP are still challenging because of the various driving factors and the intricate mechanisms influencing the production of terrestrial vegetation. Therefore, a new perspective was adopted to study the effects of urbanization and climate change on NPP in the Qinghai–Tibet Plateau in China during 2000–2020. The spatiotemporal analysis method was employed to investigate the impact of the night light urbanization index and climate factors on NPP in different HQ regions (the HQ is divided into five levels, with each area type corresponding to a specific HQ level). Then, the coupled coordination model (CCD) was used to analyze the coupling coordination relationship between NPP and HQ. Finally, the relative contribution of urbanization and climate change to NPP was studied using scenario simulation. The results showed that (1) NPP in the whole Tibetan Plateau increased very little, with an average growth rate of 0.42 g C m^{-2} per year. (2) It was surprising to find that NPP in urban areas did not decline significantly as a result of urbanization. However, there was a notable decline in NPP in higher HQ areas. (3) The mean contribution of urbanization to NPP change was found to be 17%, while the mean contribution of climate change and other factors to NPP change was 69% and 14%, respectively. These findings provide valuable insights into the interactions between human development and environmental factors, enhancing our comprehension of their role in the Tibetan Plateau's carbon cycle.

Keywords: NPP; urbanization; climate change; habitat quality; relative contributions; coupling coordination degree; Qinghai–Tibet Plateau

check for updates

Citation: Xia, T.; Han, L.; Ren, C.; Xu, Q.; Zhang, D.; Sun, G.; Feng, Z. Assessing the Impacts of Urbanization and Climate Change on NPP Under Different Habitat Quality Conditions over the Last Two Decades in the Tibetan Plateau, China. *Land* **2024**, *13*, 2139. https://doi.org/10.3390/land13122139

Academic Editor: Adrianos Retalis

Received: 31 October 2024
Revised: 4 December 2024
Accepted: 5 December 2024
Published: 9 December 2024

Copyright: © 2024 by the authors. Licensee MDPI, Basel, Switzerland. This article is an open access article distributed under the terms and conditions of the Creative Commons Attribution (CC BY) license (https://creativecommons.org/licenses/by/4.0/).

1. Introduction

Net primary productivity (NPP) in vegetation represents the total accumulation of organic material within terrestrial ecosystems [1]. NPP is determined by subtracting the carbon released during respiration from the carbon absorbed during photosynthesis [2]. The productive capacity of vegetation in a natural environment is affected by climate, terrain, human factors, pathogens, etc. Plant productivity in a natural environment can be directly reflected by NPP, representing the overall quality of terrestrial ecosystems. Furthermore, NPP is essential for identifying the carbon sources and sinks within ecosystems, influencing the regulation of ecological processes, and has a significant bearing on global change

and carbon dynamics [3]. Climate change and urbanization have a profound impact on terrestrial vegetation dynamics [4,5]. Through modifications in photosynthesis, respiration, and the decomposition rates of soil organic carbon, changing climate conditions affect the productivity of terrestrial vegetation [6]. On the other hand, the urbanization process, especially the land use and cover change during urbanization [7], has directly changed the structure of terrestrial vegetation and destroyed the production process and function. The results of recent studies indicate a significant relationship between habitat quality (HQ) and NPP. Therefore, it is crucial to identify the mechanisms through which urbanization and climate change affect NPP in different HQ contexts [8].

NPP evaluation methods range from field measurements to model-based simulations. While field measurement methods can help produce more accurate local data, making measurements on regional and time scales remains a challenge. To overcome these limitations, model-based NPP simulations have been widely used at regional [9], national [10], and global scales [11]. Its advantage is that accurate carbon exchange information can be obtained on a larger spatial scale [12]. Among the current popular models [13], the Carnegie Ames Stanford Approach (CASA) model has the advantages of high computational efficiency and easy integration of vegetation parameters and climate factors in remote sensing data. It is currently the most commonly used satellite remote sensing model to assess the geographical location and vegetation type of large areas [14–16]. However, the CASA model has a high underestimation when estimating NPP [17]. Due to the high NPP of the forest area, the CASA model underestimates the NPP of this area [18]. The CASA model uses the vegetation normalization index (NDVI) to estimate NPP; however, the saturation problem of NDVI leads to inaccurate estimation of crop yield and low sensitivity under high vegetation biomass [19]. Some studies have shown that the saturation problem of NDVI can be solved by EVI, which has been proven to be more reliable under high vegetation coverage and adapted to the response of soil, canopy background signal, and climate to vegetation [20]. Therefore, it is feasible to replace NDVI with EVI in high vegetation biomass areas.

An effective scientific evaluation of how ecosystems respond to climate change and urbanization is crucial for the formulation of informed policies. [21]. Since the 1980s, the global trend in NPP has indicated an upward trajectory; however, there are large differences in spatial drivers [22,23]. In recent decades, the regional NPP in China has been constantly changing due to climate change, and urbanization has gradually become an important factor in the change of NPP [24–26]. Second, NPP under different conditions responds differently to climate change and urbanization. Furthermore, the mechanisms by which climate change and urbanization contribute to NPP vary significantly across different time periods [27–29]. Consequently, it is essential to further investigate the factors influencing changes in NPP across different regions and timeframes within the conditions of globalization. The relationship between habitat quality (HQ) and biodiversity has always been a key area of ecological research, and a large number of studies have shown that high HQ can significantly promote the richness and stability of biodiversity [30]. In recent years, the impact of HQ on vegetation NPP has gradually received attention. Studies have shown that high HQ not only supports plant growth and improves photosynthetic efficiency by providing a suitable ecological environment, but also promotes the improvement of NPP, and further optimizes habitat conditions through the ecological function feedback of vegetation. Thus, a virtuous cycle is formed within the ecosystem [31]. At the same time, the increase in NPP also provides basic support for maintaining HQ, for example, by increasing soil organic matter content and improving microclimate conditions, further improving the ecological carrying capacity and suitability of habitats [32]. A thorough understanding of the multifaceted impacts of HQ degradation on ecosystem function and NPP can not only provide a scientific basis for decision-makers but also guide the development of rational natural resource conservation and use strategies. By improving the quality of habitat, the normal operation of ecosystem functions can be more effectively maintained, and the resilience and sustainable development of the overall ecosystem can

be promoted [33]. In particular, in the context of global climate change and frequent disturbances from human activities, the protection and restoration of high-quality habitats contribute to enhancing the carbon sink capacity of ecosystems and mitigating the effects of climate change. Although independent research on HQ and NPP has achieved a lot of results, the comprehensive analysis of the interaction between the two and their dynamic relationship in the complex ecological environment is still relatively limited, especially in the rapid development of urbanization and the increasingly prominent contradiction between ecological protection needs, the relevant research is even scarcer. In this context, clarifying the interaction mechanism between HQ and NPP is not only of great significance for improving ecosystem service functions but also provides an important theoretical basis and practical guidance for achieving a balance between ecological protection and economic development [34]. Assessing the interaction of different drivers on NPP is an important goal of studying NPP, which helps to enhance our understanding of the mechanisms behind these changes. However, assessing the impacts of climate change and urbanization on NPP is challenging because of the various driving factors and the intricate mechanisms influencing terrestrial vegetation production. Some scientists have attempted to calculate the relative contributions of urbanization and natural changes to vegetation NPP [35–37]. Typically, there are two main approaches to accomplish this. The first involves using regression equations to establish correlations between temporal and spatial changes in NPP and its influencing factors, enabling an evaluation of the significance of each factor [38]. The second method is scenario simulation, which estimates the effects of climate change by comparing the actual NPP trends with those predicted under constant climate conditions. Another scenario assesses the influence of human activities by contrasting the observed NPP with the projected trend under stable human conditions [39]. However, due to the lack of reliable assessment methods, the relative effects of climate change and urbanization on spatial changes in NPP are unknown.

The Qinghai–Tibet Plateau, located in the southwestern region of China, features a rich diversity of plant species, intricate vegetation types, and distinct geographical variations. This region encompasses extensive areas of forests, snow, ice, and grasslands, playing a crucial role as both a starting point and a regulatory zone for climate change in the Northern Hemisphere [40]. Characterized by a subtropical monsoon climate typical of plateau mountain regions, the Qinghai–Tibet Plateau's alpine ecosystem exhibits greater sensitivity to global climate change compared to other areas [41]. Over the last two decades, the expansion of the economy and tourism has led to a rise in the frequency of human activities on the Qinghai–Tibet Plateau [42]. The processes of urbanization and climate change have resulted in a reduction in HQ and biodiversity loss, which has a detrimental impact on the health and stability of eco-systems, regulating the level of NPP. Therefore, it is necessary to combine the urbanization and climate multiple factors that affect the HQ in order to study the effects of urbanization and climate change on NPP in the Qinghai–Tibet Plateau.

The research objectives of this paper are as follows: (1) The characteristics of NPP's spatial-temporal variation and the relationship between habitat quality and NPP across the Qinghai–Tibet Plateau from 2000 to 2020 under varying habitat quality conditions; (2) To reveal the effects of urbanization and climate on NPP under different HQ conditions; (3) Evaluate the contributions of urbanization and climate change to changes in NPP across various habitat quality conditions, ranging from pixel-level analysis to regional assessments. Investigating these topics will enhance our understanding of the connections between changes in NPP, climate, human activities, and the interactions between NPP and habitat quality. This study is intended to provide a theoretically sound basis for preserving and developing the environment in a sustainable manner.

2. Data and Methods

Firstly, the NPP for the Qinghai–Tibet Plateau was calculated from 2000 to 2020 using the modified CASA model, and the simulated NPP was validated using the FLUXNET and ChinaFlux ground observation datasets, as well as MODIS NPP data. The HQ was

then calculated by employing the InVEST model, taking into account the impacts of disparate threat sources and their associated weights on CLCD. Subsequently, the coupling coordination degree (CCD) model is utilized to evaluate the coupling coordination between NPP and HQ. Furthermore, the Pearson correlation and F-test methods were employed to examine the correlation and significance between NPP and urbanization, as well as between NPP and climate factors under various HQ conditions. Finally, scenario simulation was utilized to assess the impacts of urbanization and climate change on NPP under different HQ conditions. The technology is shown in Figure 1.

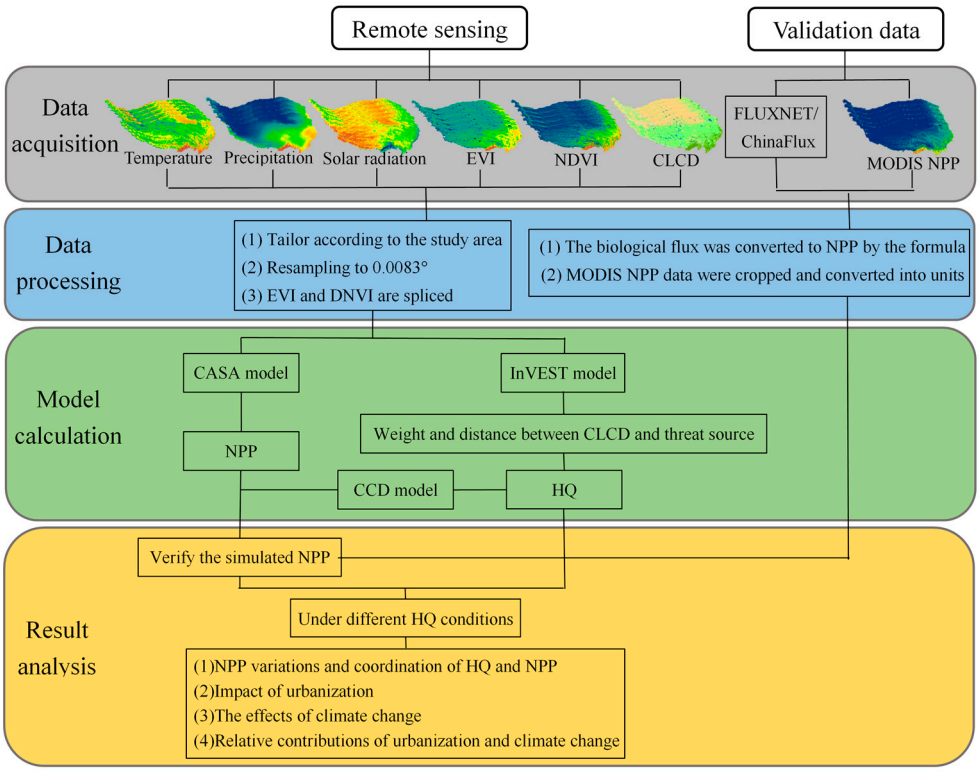


Figure 1. The technology roadmap includes four parts: data acquisition, data processing, model calculation, and result analysis.

2.1. Study Area

The Qinghai–Tibet Plateau is situated within the geographical coordinates of 26°00′12″–39°46′50″ N and 73°18′52″–104°46′59″ E and covers an area of approximately 2.615 million square kilometers. As shown in Figure 2, this vast region predominantly includes the entire Tibet Autonomous Region and Qinghai Province, along with parts of the western province of Sichuan, the southern region of Xinjiang Uygur Autonomous Region, and parts of the provinces of Gansu and Yunnan [43]. As the largest plateau in China, the Qinghai–Tibet Plateau has an average elevation exceeding 4000 m, with a general orientation from northwest to southeast [44]. Due to the high altitude, the air is relatively dry and thin, and the average annual temperature inside is lower than 0 °C; temperatures decrease progressively as elevation rises. Additionally, there is significant variability in average annual precipitation, which increases from less than 50 mm in the northwest to approximately 2000 mm in the southeast [45]. There are many plant species, complex vegetation types, and obvious geographical differences in this area. The main categories of land use include arable land, forests, grasslands, wetlands, and construction sites. In addition, the Tibetan Plateau contains vast areas of bare land, glaciers, and snow cover. In recent decades, with the rapid development of the economy and tourism, human activities on the Tibetan Plateau have become more frequent. At the same time, with the rapid increase in population in the Qinghai–Tibet Plateau, the process of urbanization

on the plateau has also developed rapidly. From 2000 to 2020, the urban population of Qinghai Province and Tibet Autonomous Region increased from 2.3 million to 4.47 million, an increase of 94.3 percent. During the same period, the gross domestic product (GDP) of Qinghai Province and Tibet Autonomous Region increased from 38.15 billion yuan to 490.86 billion yuan, an increase of nearly 12 times [46].

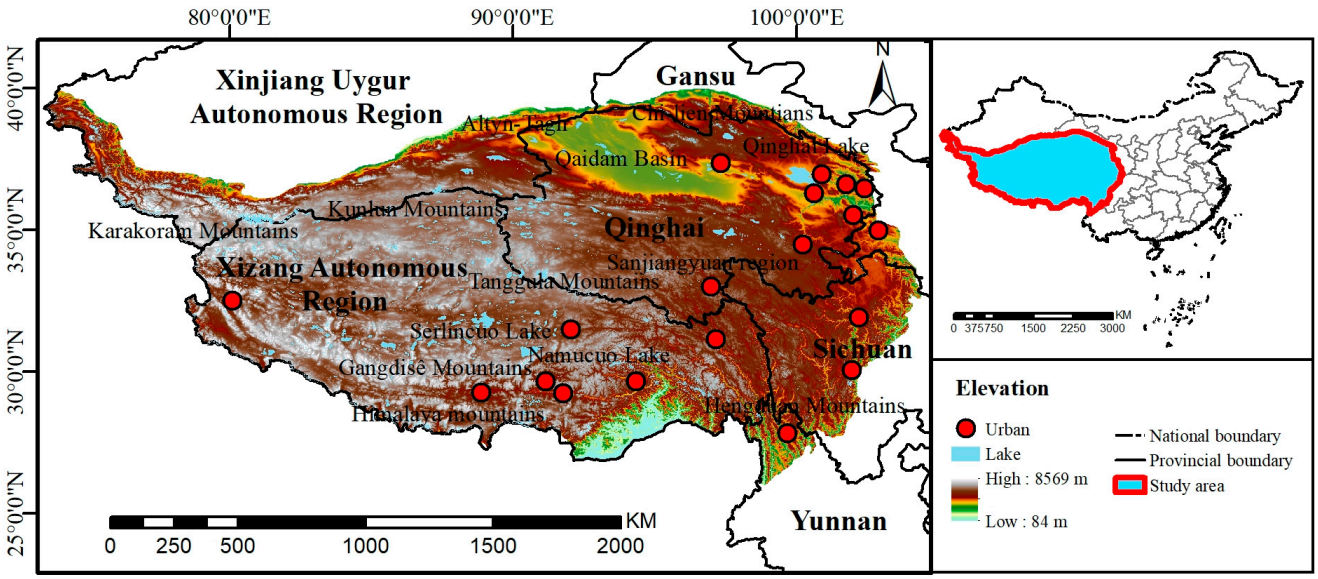


Figure 2. The location of the study area, the elevation change, and the urban distribution are represented by the red dots. A gradient from green to white indicates an increase in elevation.

2.2. Data Sources and Processing

2.2.1. Remote Sensing Data for NPP Calculation and Influence Factor

The NDVI data from MOD13A3 (https://search.earthdata.nasa.gov/search, accessed on 3 January 2024), with a spatial resolution of 1 km, was employed to calculate NPP using the CASA model (Section 2.3). The monthly EVI grid data obtained from Wuhan University (https://figshare.com, accessed on 20 January 2024) based on the Long Short-Term Memory (LSTM) neural network method from Moderate Resolution Imaging Spectroradiometer (MODIS) surface reflection rate data at 0.25° was employed to calculate NPP in vegetated areas, with density calculated using the enhanced CASA model (Section 2.3). The climate factors that affect NPP were selected as monthly temperature data sourced from the National Earth Sciences Data Center (https://www.geodata.cn, accessed on 4 January 2024), lunar radiation data from the National Earth Sciences Data Center (https://www.geodata.cn, accessed on 4 January 2024), and monthly precipitation obtained from the National Scientific Data Center of the Qinghai–Tibet Plateau (https://data.tpdc.ac.cn, accessed on 5 January 2024). The CLCD obtained from Zenodo (https://zenodo.org/records/5210928, accessed on 7 January 2024) was used to calculate HQ (Section 2.4.2). The data coordinate system of CLCD was WGS-84, and the overall accuracy reached 80%. The DMSP-OLS data set, utilizing pseudo-constant pixel calibration (https://dataverse.harvard.edu, accessed on 7 March 2024), was employed as an indicator of urbanization (Section 2.4.1). All of the data were resampled at a resolution of 0.083° in order to facilitate subsequent analysis. A brief description, unit, and time of the data are given in Table 1.

Table 1. The brief description, unit, and time of the data.

Serial Number	Data Name	Brief Description	Unit	Time
1	NDVI	Monthly data, from the MOD13A3 dataset, for CASA model NPP calculations	1 km	2000–2020
2	EVI	Wuhan University based on MODIS monthly Long Short-Term Memory (LSTM) data for NPP calculations	0.25°	2000–2020
3	Temperature	Monthly data from the National Earth Sciences Data Center for NPP calculations and impact factor analysis	0.0083333° (about 1 km)	2000–2020
4	Precipitation	Qinghai–Tibet Plateau National Scientific Data Center, monthly data for NPP calculation and impact factor analysis	0.0083333° (about 1 km)	2000–2020
5	Solar radiation	Monthly data from the National Earth Sciences Data Center for NPP calculations and impact factor analysis, verified against data from multiple sites	0.05°	2000–2020
6	CLCD	Obtained by Zenodo, this dataset is based on the Google Earth Engine for NPP calculations and habitat quality calculations	30 m	2000–2020
7	DMSP	Paper from the IEEE Journal of Earth Sciences and Remote Sensing used as an indicator of urbanization	1 km	2000–2020
8	NPP	8 days of NPP data (MOD17A3) provided by NASA for CASA model validation	0.0083°	2000–2020
9	FLUXNET data set	Field-measured data for CASA model validation		2003–2005
10	ChinaFlux data set	Field-measured data for CASA model validation		2003–2010, 2012–2016

2.2.2. NPP Verification Data

The NPP dataset obtained from NASA (MOD17A3) was used to validate the simulated NPP by the improved CASA model (https://lpdaac.usgs.gov/product_search/, accessed on 3 July 2024). The field measurement NPP data were collected from both the FLUXNET database (https://fluxnet.org/data/fluxnet2015-dataset/, accessed on 5 August 2024) and the ChinaFlux database (http://www.nesdc.org.cn/theme/index?projectId=64e80ed07e2817429fbc7b09, accessed on 5 August 2024). The FLUXNET dataset directly gives the total primary production (GPP) data of the coordinate system where the site is located, and the NPP value is calculated based on the GPP data. The two datasets were combined by treating each site's annual data as a single entity. The year of the field measurement of NPP was aligned with the year of the estimated NPP, and the spatial resolution of the estimated NPP was resampled to 3 km using bilinear interpolation. These two datasets were used to verify the improved CASA model [47].

2.3. NPP Calculation Method

Most satellite-derived NPP models posit a strong correlation between plant productivity and the amount of solar radiation that is intercepted [48]. The CASA model estimates NPP based on light utilization efficiency and has been extensively applied at both regional and global levels [49]. To accommodate local conditions, we utilize an enhanced method for estimating NPP that focuses on light utilization efficiency. This method integrates different vegetation types along with their classification accuracy into the calculation of essential vegetation parameters. More details can be found in [50]. It was found that the effect of NPP estimation is poor in forested areas because the sensitivity of NDVI data is reduced when vegetation is dense, while the sensitivity of EVI data is better in vegetated areas. Therefore, it is better to use EVI data instead of NDVI data in forest areas. The CASA model includes two essential parameters: the absorption of photosynthetically active radiation (APAR) and the light use efficiency factor (ε). The formula is as follows:

$$\mathrm{NPP}(i,t) = \mathrm{APAR}(i,t) \times \varepsilon(i,t) \quad (1)$$

where NPP(i, t) is the NPP of pixel i at time t, and APAR(i, t) and ε(i, t) are the absorption of photosynthetically active radiation and the actual light energy utilization efficiency, respectively.

$$\mathrm{APAR} = \mathrm{S(i,t)} \times \mathrm{FPAR(i,t)} \times 0.5 \quad (2)$$

where S(i, t) is the total solar radiation; FPAR(i, t) represents the proportion of green vegetation APAR; a value of 0.5 indicates the proportion of photosynthetically active radiation relative to the total solar radiation.

The following sections briefly describe the key parameters for estimating NPP (photosynthetic active radiation fraction (FPAR), maximum light use efficiency (Emax), and environmental stress).

2.3.1. Fraction of Photosynthetically Active Radiation (FPAR)

$$\mathrm{FPAP} = (\mathrm{FPAP_{VI}} + \mathrm{FPAP_{SR}}) \times 0.5 \quad (3)$$

$$\mathrm{FPAP_{VI}} = \frac{(\mathrm{VI(i,t)} - \mathrm{VI_{min}}) \times (\mathrm{FPAP_{max}} - \mathrm{FPAP_{min}})}{\mathrm{VI_{max}} - \mathrm{VI_{min}}} + \mathrm{FPAP_{min}} \quad (4)$$

$$\mathrm{FPAP_{SR}} = \frac{(\mathrm{SR(i,t)} - \mathrm{SR_{min}}) \times (\mathrm{FPAP_{max}} - \mathrm{FPAP_{min}})}{\mathrm{SR_{max}} - \mathrm{SR_{min}}} + \mathrm{FPAP_{min}} \quad (5)$$

$$\mathrm{SR(i,t)} = \left[\frac{1 + \mathrm{VI(i,t)}}{1 - \mathrm{VI(i,t)}}\right] \quad (6)$$

where VI refers to the EVI in forested regions and the NDVI in other landscapes. When $\mathrm{FPAP_{max}}$ is set at 0.950 and $\mathrm{FPAP_{min}}$ at 0.001, the highest VI value represents 95% of the VI population, while the lowest VI value corresponds to 5% of that same population.

2.3.2. Maximum Light Uses Efficiency (Emax)

Emax of vegetation is a crucial parameter for plant growth and plays a significant role in estimating NPP. Zhu et al. [51] based on Chinese forestry survey data, 690 NPP field observation sites, and climate and other remote sensing data, modified least square's function was used to simulate Emax of some of the typical types of vegetation in China. The Emax values of different vegetation types were different. Combined with the vegetation types of the Qinghai–Tibet Plateau, the cultivated land was 0.542, the forest was 0.985, the shrub was 0.429, the grassland was 0.542, and the grassland was 0.542.

2.3.3. Environmental Stresses

Two temperature scales are designed to capture the dual aspects of temperature's impact on plant growth:

$$\mathrm{T_\varepsilon(i,t)} = \mathrm{T_{\varepsilon 1}(i,t)} \times \mathrm{T_{\varepsilon 2}(i,t)} \quad (7)$$

$\mathrm{T_{\varepsilon 1}}$ sets the limits for adaptation, illustrating that the natural biochemical constraints of photosynthesis reduce NPP at extreme temperatures. Conversely, $\mathrm{T_{\varepsilon 2}}$ reflects how vegetation adapts to the specific seasonal temperature fluctuations typical of its surroundings.

$$\mathrm{T_{\varepsilon 1}(i,t)} = 0.02 \times \mathrm{T_o(i)} - 0.005 \times [\mathrm{T_o(i)}]^2 + 0.8 \quad (8)$$

$\mathrm{T_o(i)}$ represents the mean temperature (°C) recorded in the month with the highest VI.

$$\mathrm{T_{\varepsilon 2}(i,t)} = \frac{1.184}{\{1 + \mathrm{e}[0.2 \times (\mathrm{T_o(i)} - 10 - \mathrm{T(i,t)})]\}} \times \frac{1}{\{1 + \mathrm{e}[0.3 \times (-\mathrm{T_o(i)} - 10 + \mathrm{T(i,t)})]\}} \quad (9)$$

where T(i, t) denotes the mean temperature for each month.

The water scalar is calculated on a monthly basis, defined as the ratio of estimated evapotranspiration ($E(i,t)$) to potential evapotranspiration ($E_p(i,t)$) [9]:

$$W_\varepsilon(i,t) = 0.5 \times \frac{E(i,t)}{E_p(i,t)} + 0.5 \quad (10)$$

2.4. Calculation of Urbanization and Habitat Quality Indicators

2.4.1. Urban Sprawl Mapping

The average Night Light map generates a cloud-free composite image that represents the average light digital number (DN) for each time period from 2000 to 2020, featuring a spatial resolution of 1 km. Nighttime images obtained from DMSP/OLS are crucial for tracking urban expansion over various temporal and spatial scales [52,53]. The urban area is identified based on a specified DN threshold. If the DN in a given area exceeds this threshold, it is classified as urban. By changing the threshold of DN, different scenarios of the urban area. When the simulation of the urban area aligns closely with the urban land use census data, the corresponding DN threshold is recorded and used for mapping the urban sprawl process.

2.4.2. Calculation of Habitat Quality

From 2000 to 2020, habitat quality (HQ) in the Tibetan Plateau area was assessed every five years using the InVEST HQ model. The HQ model relies on the relative sensitivity to various threat sources, considering both their distance and weight, to establish the connection between land use types and these threats for calculation purposes [54]. The calculation formula is:

$$HQ_{ij} = H_j \left(1 - \left(\frac{D_{ij}^x}{D_{ij}^x + m^x}\right)\right) \quad (11)$$

where H_j represents the suitability of habitat for land use type j, while D_{ij}^x denotes the overall threat level associated with network pixel i under that specific land use. Additionally, m is defined as the half-saturation constant.

According to the research of other scholars, HQ is divided into five levels [55]. Table 2 shows the name of the area divided into HQ and the scope of HQ.

Table 2. Divide the name and HQ range of the five areas.

Region Name	HQ Range
Extremely low HQ area.	0–0.2
Low HQ area	0.2–0.4
Medium HQ area	0.4–0.6
High HQ area	0.6–0.8
Extremely high HQ area.	0.8–1.0

2.5. Method for Assessing the Impacts of Urbanization and Climate Change on NPP Under Different HQ Conditions

2.5.1. Coupling Coordination Degree Model

The Coupling Coordination Degree (CCD) model integrates the concepts of coupling degree and coordination degree. The coupling degree describes the dynamic interactions among several systems and provides an effective indication of the level of their interrelationship. The degree of coordination refers to the positive coupling relationships between different systems, reflecting the synergistic effects that occur between them [56,57]. Consequently, the CCD model illustrates the degree of mutual constraint and interdependence between two or more distinct systems [58]. Thus, it is an effective tool for assessing the

overall balanced level of development of the study area [59]. The interaction between NPP and HQ was quantified using the CCD method. The calculation formula is:

$$C = 2 \times \left(\frac{NPP \times HQ}{(NPP + HQ)^2} \right)^{\frac{1}{2}} \quad (12)$$

$$T = i \times NPP + j \times HQ \quad (13)$$

$$CCD = (C \times T)^{\frac{1}{2}} \quad (14)$$

where C is the coupling level, NPP and HQ are the normalized indexes of both, T is the comprehensive evaluation score, and i and j are the weight coefficients of NPP and HQ. Considering that NPP and HQ are equally important in the ecosystem, $i = j = 0.5$ [60]. The CCD represents the level of coupling coordination between NPP and HQ.

2.5.2. Calculating the Relationship Between Driving Factors and NPP Variation

All spatial datasets were produced at a uniform resolution of 1 km. Utilizing a linear regression approach for each pixel, this study examined the trends of NPP, annual temperature, annual precipitation, and annual solar radiation across the Qinghai–Tibet Plateau from 2000 to 2020. The interannual rate of change is determined by the slope of the regression line for each individual pixel. Subsequently, the Pearson correlation coefficient is computed to evaluate the relationships between each NPP-climate pair and each NPP-urbanization pair [61]. The formula is as follows:

$$R = \frac{\sum_{i=1}^{n}(y_i - \overline{y})(x_i - \overline{x})}{\sqrt{\sum_{i=1}^{n}(y_i - \overline{y})^2 \sum_{i=1}^{n}(x_i - \overline{x})^2}} \quad (15)$$

where n is the number of years during the study period, x_i is the NPP of vegetation in year i, and y_i is the value of average annual climate factors in year i.

The slope derived from the analysis reflects the importance of the observed change trend, and the F-test is utilized to determine the confidence level linked to this change. The formula is as follows:

$$\text{slope} = \frac{n \times \sum_{i=1}^{n}(i \times NPP_i) - \sum_{i=1}^{n} i \sum_{i=1}^{n} NPP_i}{n \times \sum_{i=1}^{n} i^2 - (\sum_{i=1}^{n} i)^2} \quad (16)$$

$$a = \overline{y} - b\overline{n} \quad (17)$$

$$F = (n - 2) \times \frac{U}{Q} \quad (18)$$

$$U = \sum_{i=1}^{n}(\hat{y}_i - \overline{y})^2 \quad (19)$$

$$Q = \sum_{i=1}^{n}(y_i - \hat{y}_i)^2 \quad (20)$$

where i ranges from 1 to 21, where 1 corresponds to the year 2000, 2 to 2001, and so forth. The total number of years considered, n is 21, representing the study period. NPP_i denotes the NPP value for year i. Additionally, U signifies the regression sum of squares, while Q indicates the sum of squared errors. The variable y_i represents the actual NPP for year i, $\hat{y}_i$ is the regression value, and $\overline{y}$ refers to the average NPP over the 21-year period. The significance of NPP changes is assessed using the F-test, with a threshold of ($p < 0.05$).

2.5.3. Calculating the Relative Contributions of Climate Change and Urbanization to NPP

The fluctuations and dynamics of NPP are shaped by a combination of natural changes and human activities [62]. Identifying the effects of urbanization and climate on NPP changes, distinct from other influencing factors like fertilization, nitrogen deposition, and agricultural practices, is essential [63]. Evaluating the NPP considers two scenarios. In the first scenario, we predict the NPP by taking into account the changing climate without urban development. Here, we suggest that land designated for urban and peri-urban use can have an annual NPP level comparable to that of non-urban areas. Building on this, the VI for the urban expansion area from 2000 to 2020 is substituted with the VI from 2000. In the second scenario, we utilize the average monthly precipitation, temperature, and solar radiation data from 2000 to 2020 to assume a stable climate while accounting for changes in vegetation [37,64].

The impact of urbanization on NPP (ΔU.NPP) was assessed by computing the difference between the slope of the observed NPP and the slope predicted under a scenario of stable urbanization. Similarly, the influence of climate on NPP (ΔC.NPP) was evaluated through a simulation that preserves constant climatic conditions. The residual indicates the difference between the slope of the observed NPP and the combined slopes from simulations accounting for both constant urbanization and climate. The residual captures the influences that remain unaddressed by the effects of climate change and urbanization [65]. As a result, the impact of climate change, urbanization, and additional unexplained factors on variations in NPP can be expressed through the equations presented below:

$$\text{Contr.U} = \frac{|\Delta\text{U.NPP}|}{|\Delta\text{U.NPP}| + |\Delta\text{C.NPP}| + |\text{Residual}|} \times 100\% \quad (21)$$

$$\text{Contr.C} = \frac{|\Delta\text{C.NPP}|}{|\Delta\text{U.NPP}| + |\Delta\text{C.NPP}| + |\text{Residual}|} \times 100\% \quad (22)$$

$$\text{Contr.R} = 100 - \text{Contr.U} - \text{Contr.C} \quad (23)$$

The total contribution of city, climate, and residual factors is 1. Each of these three impact factors can be individually mapped at the pixel level, allowing for the creation of a synthesized image through a Maxwell Triangle.

3. Results

3.1. NPP Calculation and Validation

The NPP product for the Tibetan Plateau was simulated at a resolution of 0.083° over the past two decades using an improved CASA model. The in situ sites (28 sites) were collected to validate the NPP simulated using the modified CASA model with $R^2 = 0.65$, $p < 0.05$, RMES = 57.3 g Cm^{-2} (Figure 3a). Due to the scarcity of field-measured data in forest improvement areas [66], MODIS products were used to validate the NPP simulated from the CASA model and improved CASA model. The NPP simulated from CASA model showed good consistency with MODIS NPP products ($R^2 = 0.82$, $p < 0.05$, RMES = 111.6 g Cm^{-2}) (Figure 3b). Nevertheless, as the NPP increases, particularly in areas with dense vegetation, the margin of error in NPP calculations is correspondingly higher. The improved CASA model also showed a high correlation with MODIS products ($R^2 = 0.81$, $p < 0.05$, RMES = 112.6 g Cm^{-2}) (Figure 3c), spatially in dense vegetation areas.

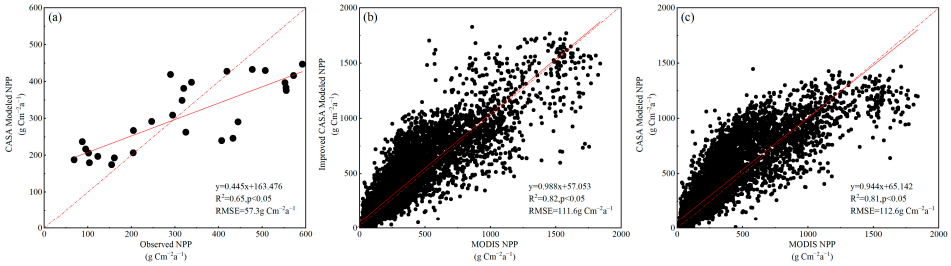


Figure 3. Enhance the correlation between CASA-simulated NPP and field-measured NPP (**a**), strengthen the connection between CASA-simulated NPP and the MODIS NPP dataset (**b**), and refine the association between CASA-simulated NPP and the MODIS NPP dataset (**c**). The red line is a linear fit line, and the virtual red line is a 1:1 line.

3.2. NPP Variations Under Different HQ and Coordination of HQ and NPP

Qualitative changes in habitat quality reflect ecosystem responses to adverse factors, thereby influencing net primary productivity. The spatial heterogeneity of habitat quality decreases significantly from southeast to northwest, categorizing habitat quality into five levels (Figure 4). These five categories include extremely low HQ, low HQ, medium HQ, high HQ, and extremely high HQ areas. Regions with higher HQ values indicate better ecological conditions, while areas with lower HQ values signify poorer habitat quality. Low HQ areas are predominantly found in barren lands, western grasslands, and southern river valleys. In contrast, high HQ areas are mainly located in the forested regions of the southeastern Qinghai–Tibet Plateau (Figure 4). Many habitats in the study area have shown a declining trend, with the most severely affected regions concentrated in the western Tibetan Plateau, northern Gangdisê, and southern Kunlun Mountains (Figure S1).

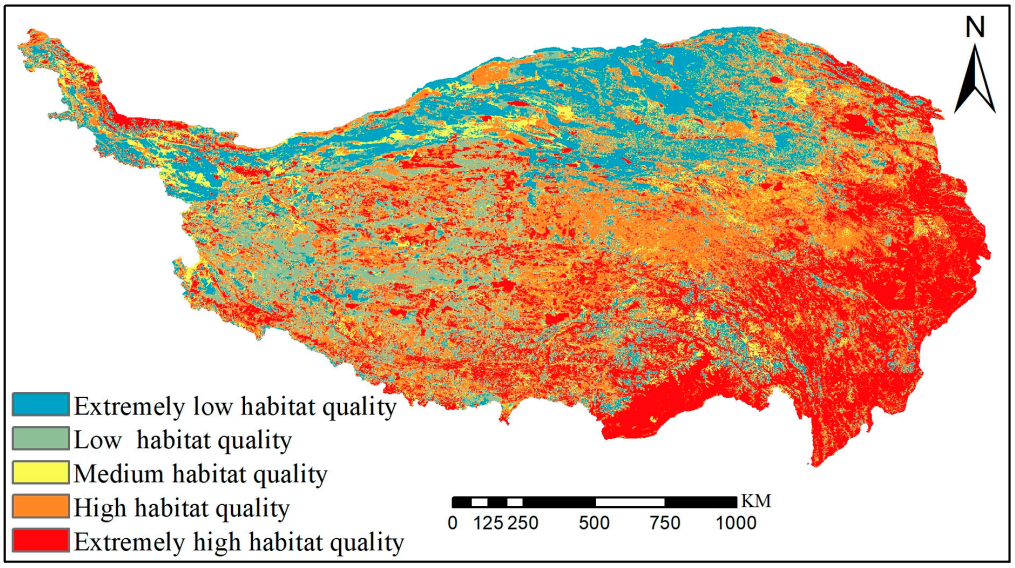


Figure 4. Habitat quality was calculated using the InVEST model, averaging habitat quality from 2000–2020 in five classes.

During the study period, NPP showed a slight increase, with a change rate of 0.42 g C m^{-2} per year (Figure 5). As illustrated in Figure 5, NPP trends varied across different habitat qualities. Based on the varying levels of habitat quality in the study area, as well as the trends and significance of NPP changes, the analysis was categorized into five distinct regions. Overall, NPP exhibited a slight decline of 0.15 g C m^{-2} per year in the extremely high HQ area while increasing in other regions.

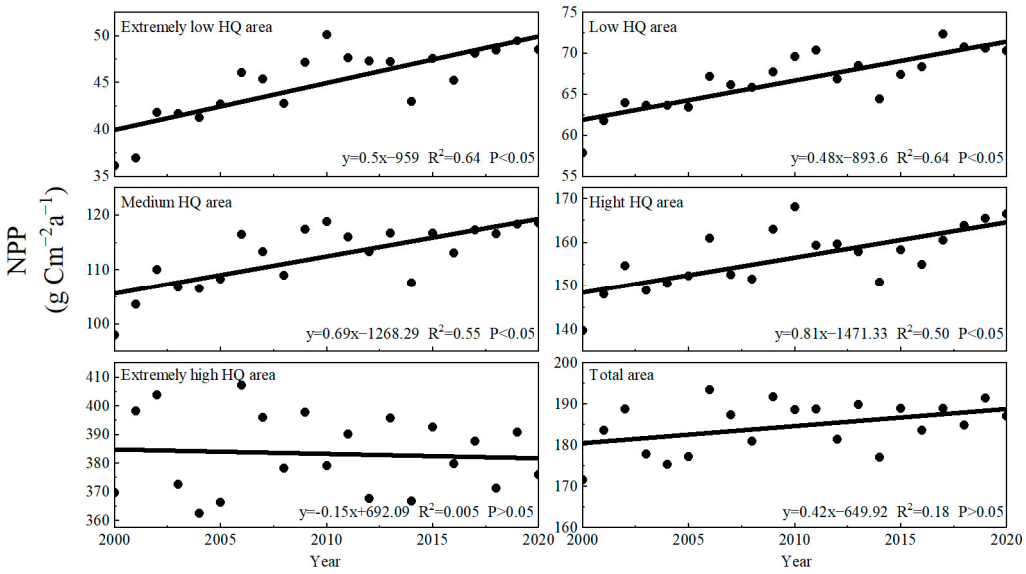


Figure 5. Trends of NPP at different HQ levels on the Tibetan Plateau from 2000 to 2020. The solid line represents the linear fit for the period 2000 to 2020.

To examine the spatial distribution of NPP changes, the trend of NPP variation from 2000 to 2020 was analyzed at the pixel level. As shown in Figure 6, NPP increased in 79.1% of the study area, with 40.7% showing a significant increase ($k > 0$, $p < 0.05$; k value plus or minus represents positive or negative slope, $p < 0.05$ indicates significant, $p > 0.05$ indicates no significant). Approximately 20.9% of the area exhibited a decrease in NPP, with 16.7% showing a significant decline ($k < 0$, $p < 0.05$). The spatiotemporal patterns of NPP varied across the five sub-regions. In areas with extremely low, low, moderate, and high HQ, more than 80% of the area showed an increasing NPP trend (Figure 6). In the extremely low HQ region, significant increases in NPP were primarily concentrated around the Qaidam Basin [67], while a significant decrease in NPP occurred in the basin's central area (Figure S4). In the low HQ region, areas with significant increases were mainly located from the southern part of the low HQ zone to the northern Gangdese Mountains (Figure S4). Areas with no significant increase were primarily found in the northern part of the low HQ zone (Figure S4). In the moderate HQ region, increased NPP areas were mostly in the northern part, with significant increases concentrated in the southern part of the region (Figure S4). In the high HQ region, significant increases were mainly observed in the Sanjiangyuan area (Figure S4). Significant decreases were concentrated around the Namucuo and Selincuo lakes (Figure S4). In the extremely high HQ region, 63.2% of the area showed an increasing NPP trend, with 40.4% showing a significant increase ($k > 0$, $p < 0.05$), while 26.4% showed a significant decrease ($k < 0$, $p < 0.05$) (Figure 6). The extremely high HQ region, primarily located in the southeastern Qinghai–Tibet Plateau and dominated by forest vegetation, showed a substantial NPP decrease along the southeastern side of the Himalayas, particularly in the border areas of India and Bangladesh. A similar trend was observed in the eastern Qinghai–Tibet Plateau and the Sichuan border areas. In contrast, the southwestern slope of the Hengduan Mountain Range in Yunnan also showed a significant NPP decrease (Figure S4).

The coupling coordination level serves as a measure of the relationship between NPP and HQ [68]. As shown in Figure S2, the coupling coordination degree between total HQ and NPP decreases from southeast to northwest. Throughout the study period, coordination in the southeastern, highly coordinated region improved, while coordination in the northwestern, uncoordinated region worsened (Figure S2f). The overall change in coupling coordination for the study area was −0.0009 per year ($p < 0.05$), with the increase in the southeastern region offsetting the decrease in the northwestern region, resulting in no significant overall change. During the study period, significant differences were observed in the coupling coordination

changes across regions with different habitat qualities. In the extremely low and low HQ regions, large areas shifted toward severe imbalance (Figure 7a,b). In the moderate HQ region, the shift remained relatively balanced (Figure 7c). In the high and extremely high HQ regions, the coupling coordination degree in large areas shifted from imbalance to balance (Figure 7d,e). These results suggest that in low HQ areas, the coupling coordination degree gradually became imbalanced, leading to ecosystem instability, while in high HQ areas, the coordination degree moved toward balance.

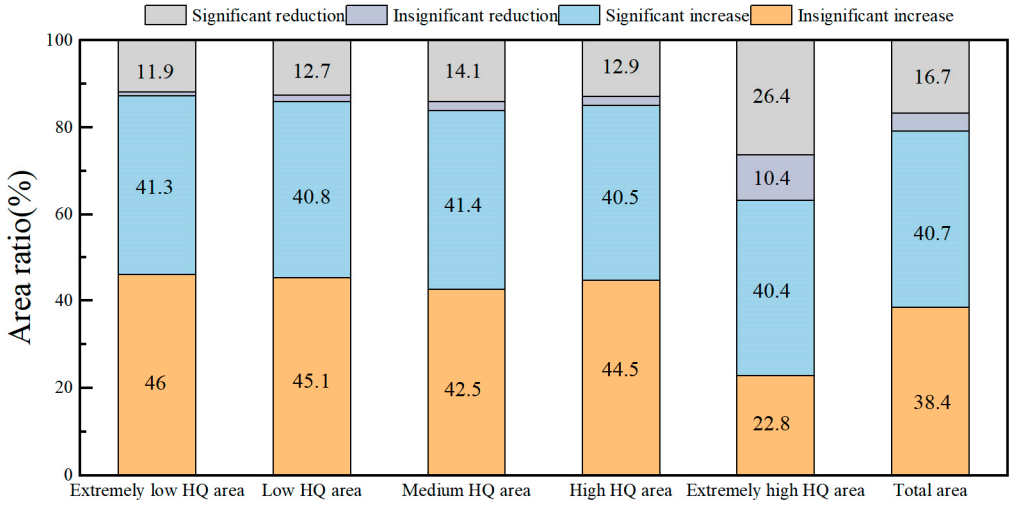


Figure 6. Percentage of significance of changes in vegetation NPP under different HQ from 2000 to 2020.

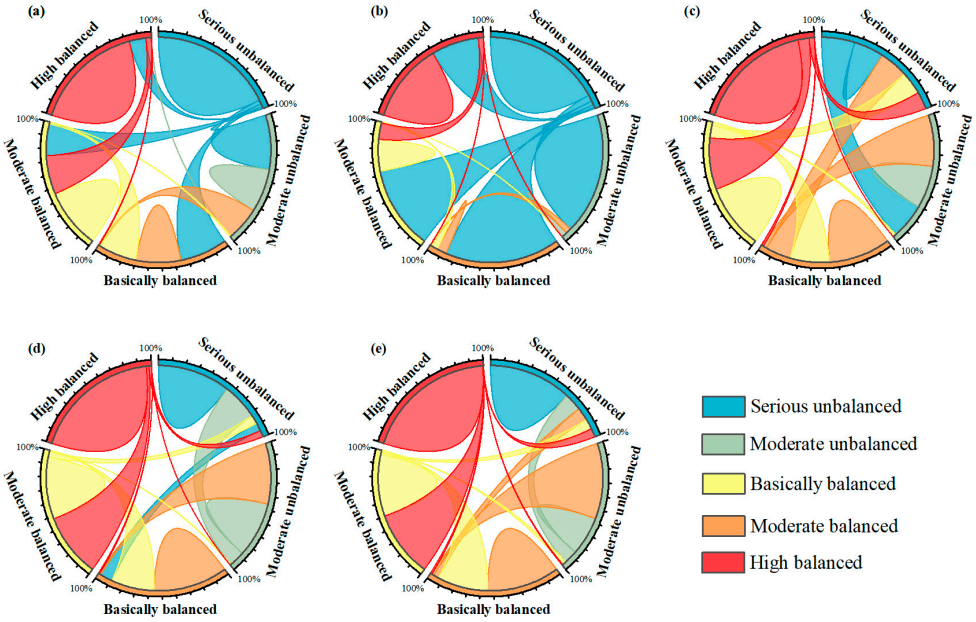


Figure 7. Shift plots of NPP and HQ coupling coordination under different HQ classes from 2000 to 2020. (**a**) Extremely low HQ area; (**b**) low HQ area; (**c**) medium HQ area; (**d**) high HQ area; (**e**) extremely high HQ area.

3.3. Urbanization Process and Its Influence on NPP Change Under Different HQ

3.3.1. Urbanization Process

In 2000, the Qinghai–Tibet Plateau had a permanent population of 10.07 million, with an urban population of 2.51 million, resulting in an urbanization rate of 24.87%. By 2020, the permanent population and urban population of the plateau had increased to 12.50 million and

5.94 million, respectively, with the urban population accounting for 47.53% of the total [69]. During this period, the area of urban construction expanded nearly threefold, and the length of highways grew more than fourfold. The urban population grew from 2.51 million to 5.94 million, and the urbanization rate rose from 24.87% to 47.53%, reflecting an annual growth rate of 1.1% [70]. According to the seventh national population census, scheduled for release in 2021, the total permanent urban population in the Qinghai–Tibet Plateau study area is projected to be 78.78 million, with 43.29 million permanent urban residents, resulting in an urbanization rate of 54.95%. The GDP per capita in the region has shown consistent growth, surpassing 10,000 yuan in 2006, with a more pronounced growth trend since 2010 [71]. These trends indicate that the processes of urbanization and industrialization on the Tibetan Plateau are expected to continue over the next decade.

Based on the nighttime light index derived from DMSP/OLS images (Figure 8), significant transformations have occurred in the cities of the Tibetan Plateau, particularly in Xining, Geermu, and Lhasa, where rapid urbanization is evident. The urban area expanded substantially from 295.6 km^2 in 2000 to 807.6 km^2 in 2020 (Figure S5) [72], marking an increase of 723.49 km^2, or 1.7 times the original area. The urban area grew at an average rate of 24.4 km^2 per year between 2000 and 2020.

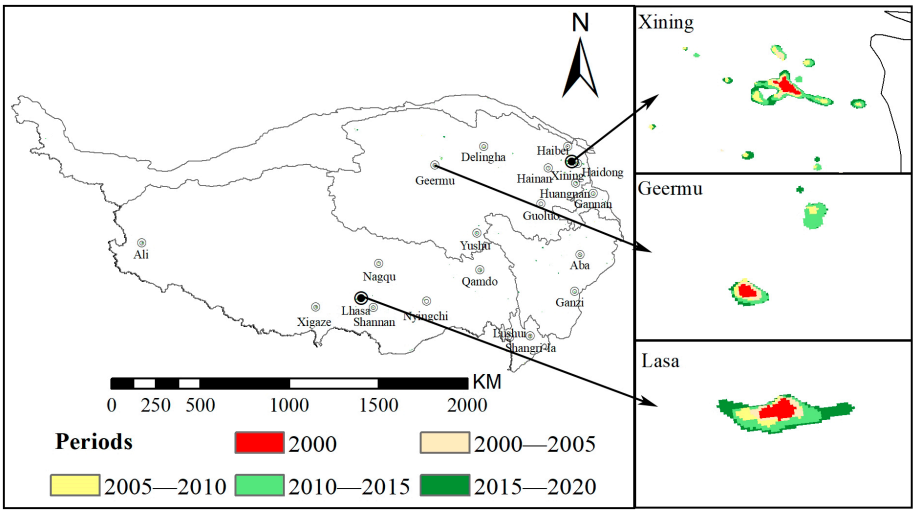


Figure 8. Urban sprawl on the Tibetan Plateau from 2000 to 2020 was detected using nighttime lighting data. This period is divided into four periods of five years each. Xining, Lasa, and Geermu are the top three cities on the Tibetan Plateau.

3.3.2. Impact of Urbanization on NPP Change Under Different HQ

The nighttime light index serves as an indicator of urbanization, with areas where light intensity exceeds a certain threshold defined as urban areas. A positive correlation exists between NPP and the nighttime light index (Figure S6). In regions with extremely high HQ, over 50% of urban areas show a negative correlation with NPP, and 26.2% of these regions exhibit a significant negative correlation (Figure 9). In contrast, more than 50% of regions in all other areas display a positive correlation (Figure 9). The extremely high HQ regions are primarily located in the southeastern part of the study area, where forest vegetation predominates. Urbanization exerts a more pronounced impact on these areas. Across the entire study area, 59.3% of NPP values are positively correlated with nighttime light data (Figure 9), suggesting that urbanization positively influences NPP in more than half of urban areas. Among these, 18.9% show a significant positive correlation, while 22.7% exhibit a significant negative correlation (Figure 9). NPP tends to increase in urban sprawl areas, while it tends to decrease in urban centers (Figure S3). The relationship between urban nighttime lighting and NPP from 2000 to 2020 is shown in Figure S6. For each unit increase in the nighttime light index (DN), urban NPP increases by approximately 0.38 g C m^{-2} per year.

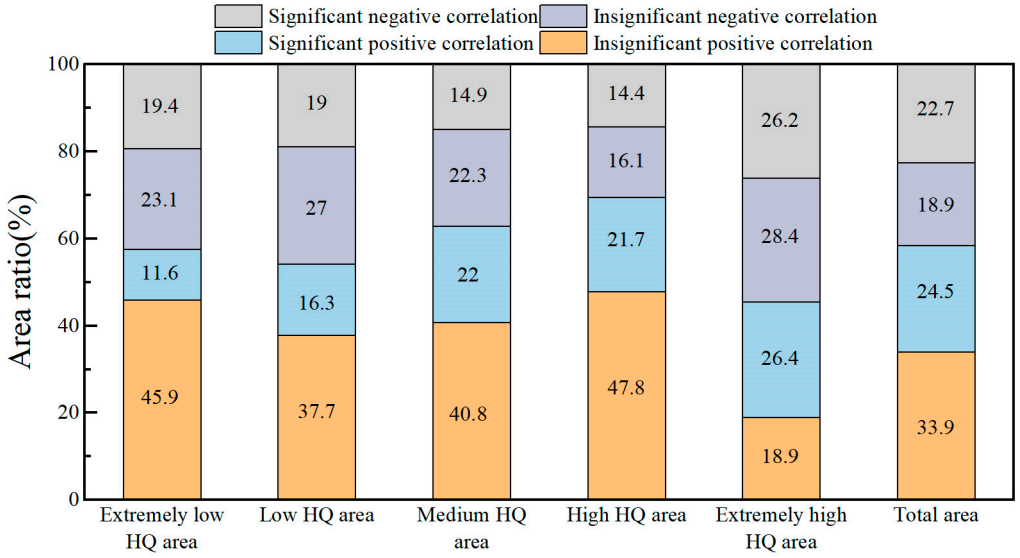


Figure 9. A plot of relative significance ratios of NPP versus nighttime light under different HQ regions.

3.4. Impact of Climate on NPP Change Under Different HQ

3.4.1. Time and Space Variations in Temperature, Precipitation, and Solar Radiation

The unique geographic location and elevation of the Tibetan Plateau make it particularly susceptible to climatic fluctuations. The region is characterized by a typical highland mountain climate, in addition to a subtropical monsoon climate [73]. Due to its high altitude and the influence of the Indian Ocean monsoon, the water vapor gradient extends from the southeast to the northwest. Studies have shown that the impacts of global warming have become increasingly evident in recent years, with the rate of temperature rise at high altitudes and latitudes exceeding the global and Northern Hemisphere averages. The climate of the Tibetan Plateau is characterized by low temperatures, high solar radiation, and distinct wet and dry seasons due to its elevation [74].

The Tibetan Plateau exhibits similar spatial distribution patterns for mean annual temperature and precipitation, with both showing a gradual decline from the southeast to the northwest. The annual mean temperature increases at a rate of 0.006 °C per year across 60% of the plateau (Figure 10d). However, a decreasing trend in temperature is observed in the Qaidam Basin, particularly in the southwestern Kunlun Mountains and the Pamir Plateau in the western part of the Plateau (Figure 10a). Other large areas show increasing temperatures, especially in the riverine regions, where the temperature rise is particularly pronounced near rivers (Figure 10a). From 2000 to 2020, precipitation increased at an annual rate of 0.056 mm (Figure S7), with nearly 70% of the region exhibiting an upward trend (Figure 10e). Xining and its surrounding areas experienced a notable growth trend, with an annual increase of 0.4 mm or more (Figure 10b). The Himalayas, Tanggula Mountains, and Hengduan Mountains, particularly along the borders with India and Myanmar, showed negative growth (Figure 10b), while the rest of the region exhibited an increasing trend (Figure 10b). The trend in solar radiation was -1.1 MJ m^{-2} per year, indicating a decrease (Figure S7), with 96% of the Plateau showing negative growth (Figure 10f). The regions experiencing positive growth were mainly concentrated in the Qaidam Basin, the southern slopes of the Hengduan Mountains, and along the Yarlung Tsangpo River and Namucuo (Figure 10c).

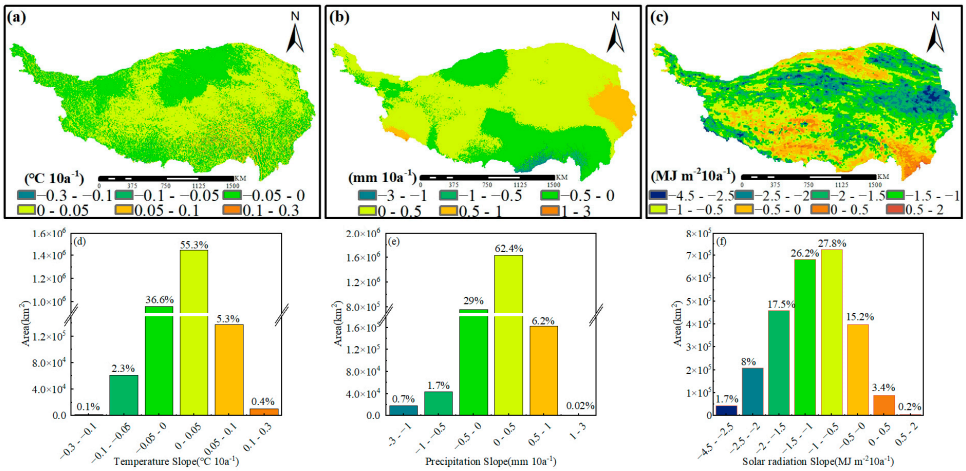


Figure 10. Spatial pattern and classification ratio of pixel resolution of climate factor growth rate. (**a**,**d**): Pixel resolution spatial pattern and classification proportion of annual temperature growth rate from 2000 to 2020; (**b**,**e**): Pixel resolution spatial pattern and classification proportion of annual precipitation growth rate from 2000 to 2020; (**c**,**f**): Pixel resolution spatial pattern and classification proportion of annual solar radiation growth rate from 2000 to 2020.

3.4.2. Impact of Climate on NPP Change Under Different HQ Regions

The pixel-by-pixel correlation analysis revealed minimal variation in the impact of temperature on NPP across different HQ conditions. Overall, temperature exhibited a positive influence on NPP at various HQ levels. In more than 74.3% of the study area, a positive relationship between NPP and temperature was observed, with 42.9% of the area showing a statistically significant positive correlation (Figure 11c). Approximately 25.7% of the region exhibited a statistically significant negative correlation with temperature, and an additional 14.6% showed a noteworthy negative relationship (Figure 11c). Negative correlations were primarily found in the Himalayas, around the two lakes, Namucuo and Selincuo, to the north of the mountain range, and at the intersection of the Kunlun Mountains and the Tarim Basin (Figure 11a,b). Between 2000 and 2020, 60% of the Tibetan Plateau exhibited a warming trend (Figure 10d), leading to an increase in NPP. In most areas, the effect of temperature on NPP was significantly correlated, highlighting temperature as a key factor influencing NPP.

Precipitation is another key factor influencing NPP. The analysis revealed that the increase in precipitation across the study area during the research period contributed to a rise in NPP. In areas with extremely low, low, medium, and high HQ, more than 60% of the region exhibited a positive correlation between NPP and annual precipitation, with nearly 40% showing a significant positive correlation (Figure 11f). In contrast, in regions with extremely high HQ, over 50% of the NPP displayed a negative correlation with annual precipitation, with 37.9% of the area showing a significant negative relationship (Figure 11f). Overall, a positive correlation was found between regional NPP and annual precipitation throughout the study area, with 60% of the region showing a positive relationship, and 31.7% reflecting a significant positive association (Figure 11f). Conversely, 25.8% of the region exhibited a significant negative correlation with precipitation (Figure 11f). In areas with extremely low, low, moderate, and high HQ, the positive correlation zones were primarily concentrated in the Sanjiangyuan region, the northeastern Tibetan Plateau, the northwestern Himalayas, and the western end of the Tanggula Mountains (Figure 11d,e). This was mainly due to lower precipitation levels in these areas. In regions with extremely high HQ, the negative correlation was primarily observed in the southern Tanggula Mountains and the southeastern Tibetan Plateau at elevations below 5000 m.

As solar radiation increases, vegetation photosynthesis is enhanced, leading to an increase in NPP [75]. Studies indicate a rising trend in solar radiation in the Northern Hemisphere over the past 20 years [76]. However, from 2000 to 2020, solar radiation in this

region showed a decreasing trend [77]. In the study area, 41.4% of the region exhibited a positive relationship between solar radiation and NPP, with 32.4% of the area showing a significant positive correlation (Figure 11i). In regions with extremely low, low, medium, and high HQ, more than 60% of regional NPP was negatively correlated with terrestrial radiation, with significant negative correlations observed in 24.2%, 28.9%, 24.7%, and 27.9% of the areas, respectively (Figure 11i). These regions with significant negative correlations were mainly concentrated north of the Himalayas, extending to the Karakoram Range and Tanggula Mountains (Figure 11g,h). Significant positive correlations were found in 29%, 24.6%, 30.7%, and 25.4% of the four regions, respectively, primarily in the Qaidam Basin and at the intersection of the Karakoram and Kunlun Mountains in the northwestern Tibetan Plateau (Figure 11g,h). In regions with extremely high HQ, 45.6% of the area exhibited significant increases in solar radiation (Figure 11i), with the concentration primarily located in the southeastern Tibetan Plateau (Figure 11g,h).

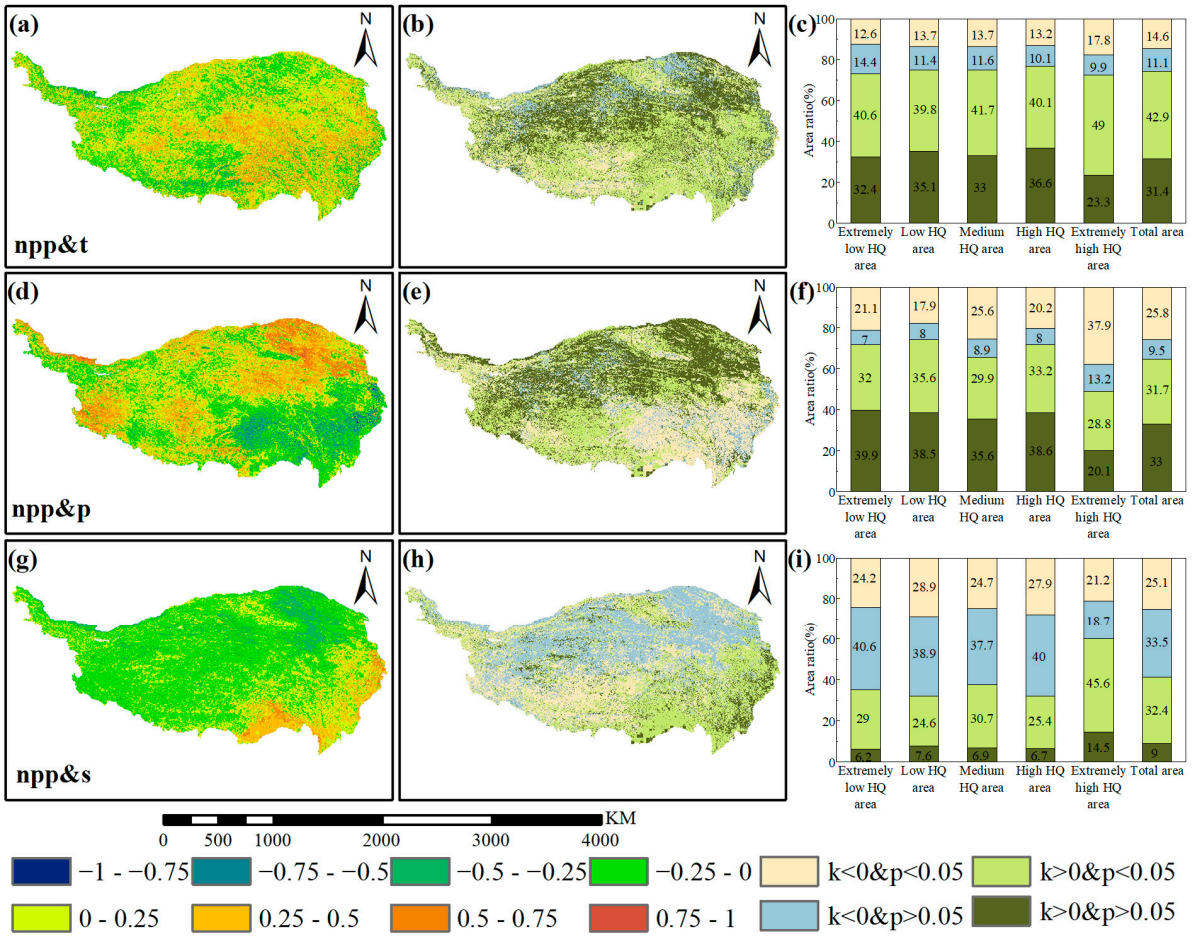


Figure 11. The spatial distribution of correlation between NPP and climate parameters, its correlation coefficient, its relative significance level spatial distribution, and significance level proportion graph from 2000 to 2020. (**a**–**c**) The correlation between NPP and temperature, the relative significance level and the proportion of significance level; (**d**–**f**) The correlation between NPP and precipitation, the relative significance level and the proportion of significance level; (**g**–**i**) Correlation between NPP and solar radiation, relative significance level graph and significance level proportion graph.

3.5. Relative Contributions of Urbanization and Climate Change Under Different HQ

The effect of urbanization on NPP (ΔU.NPP) was measured as the difference between the slope of NPP change under a sustained urbanization scenario and the simulated slope of NPP change. The mean values of ΔU.NPP were 0.18, 0.0122, 0.0122, −0.0066, and −0.0133 g C m^{-2} per year for the five HQ regions: extremely low HQ area, low HQ area, medium HQ area, high HQ area, and

extremely high HQ area, respectively. The overall mean ΔU.NPP was −0.1426 g C m^{-2} per year (Table 3), indicating that NPP loss due to urbanization on the Tibetan Plateau was −0.1426 Tg C per year. While urbanization positively influenced NPP in urban areas, it caused a declining trend in NPP across medium, high, and extremely high HQ areas. The findings suggest that urbanization had a more severe impact on areas with higher habitat quality, significantly reducing ecosystem productivity in these regions. However, urbanization was not the primary driver of NPP changes on the Tibetan Plateau, accounting for only 17% of the total drivers (Table 3). The contributions of urbanization to NPP changes in each region are detailed in Figure 12a.

Table 3. The annual change rate of NPP and the relative contribution of urbanization, climate change, and residual factors to the change trend of NPP in different HQ regions of Qinghai–Tibet Plateau from 2000 to 2020.

Items		Extremely Low Hq Area	Low HQ Area	Medium HQ Area	High HQ Area	Extremely High HQ Area	Total Area
NPP change rate (g $Cm^{-2}a^{-1}$)	ΔU.NPP	0.018	0.0122	−0.0066	−0.0133	−0.4957	−0.1426
	ΔC.NPP	0.4995	0.4778	0.687	0.8099	−0.1536	0.4152
	Residua	0	−0.0351	−0.0401	−0.1118	−0.2293	−0.1066
Contribution ratio (%)	Urban-driven	14	16	16	16	21	17
	Climatic-driven	75	71	71	70	63	69
	Residual	11	13	13	14	16	14

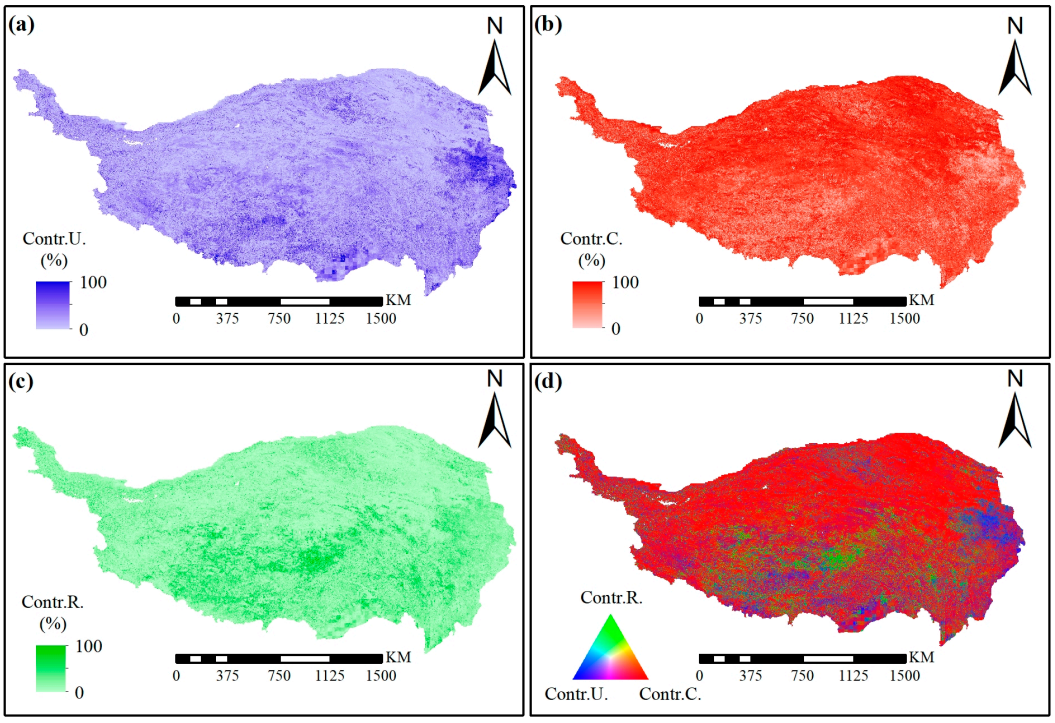


Figure 12. Spatial distribution of contributions of urbanization and climate change to NPP: (**a**) contribution of urbanization, (**b**) contribution of climate, (**c**) contribution of residual mechanisms. (**d**) Maxwell colored triangles are used to provide a visual view of the relative contributions of the three influencing factors on the map.

Moreover, ΔC.NPP for the entire Tibetan Plateau was calculated as the difference between the observed NPP slope and the simulated NPP slope under stable climate conditions (Figure 12b). As shown in Table 3, ΔC.NPP for the entire Tibetan Plateau was 0.4152 g C m^{-2} per year, with values of 0.4995 g C m^{-2} per year for extremely low HQ areas, 0.4778 g C m^{-2} per year for medium HQ areas, 0.687 g C m^{-2} per year for high HQ areas, and −0.1536 g C m^{-2} per year for extremely high HQ areas. Climate change contributed more significantly to NPP in the extremely

low, low, medium, and high HQ areas, with these four regions accounting for more than 70% of the climate's contribution (Table 3). Overall, the contribution of climate factors accounted for 69% of the total changes in NPP across the region (Table 3). Climate variables are, therefore, the primary drivers of NPP changes on the Tibetan Plateau.

Residual contributions refer to factors that cannot be explained by fluctuations in climate or urbanization. The residual contribution accounted for 14% of the total variation in NPP across the study area, suggesting that other factors are not the primary drivers of NPP changes (Figure 12c). This may be related to the concentration of CO_2, which has been observed to influence vegetation growth, particularly in water-scarce regions [78].

Maxwell's color triangle is a valuable tool for visually assessing the relative impacts of urbanization, climate change, and other influencing factors. This method offers a clear and objective way to represent the contribution of each factor on the map (Figure 12d). The analysis reveals that urbanization accounts for an average of 17% of the NPP change across the Tibetan Plateau, climate change contributes 69%, and other factors contribute 14%. Mapping these contributions spatially provides insights into the effects of human activities on terrestrial ecosystems and enhances our geographic understanding of these changes.

4. Discussion

4.1. Factors Affecting NPP Accuracy from Remote Sensing

The CASA model offers substantial computational efficiency and the convenient acquisition of parameter data. Consequently, the CASA model is currently the most widely utilized satellite remote sensing model for the assessment of NPP [14–16]. The NPP simulated from the CASA model exhibited satisfactory accuracy in areas of sparse vegetation, while the margin of error was found to be correspondingly higher in areas of dense vegetation (Figure 3b). This discrepancy may be attributed to the CASA model's reliance on the vegetation normalization index (NDVI) to estimate NPP. However, the saturation problem associated with NDVI can result in an inaccurate estimation of crop yield and low sensitivity under conditions of high vegetation biomass. In view of the findings presented in previous literature [19], a novel enhanced CASA model was proposed by substituting the input parameters NDVI with EVI in forest regions characterized by dense vegetation. The NPP calculation results from the newly improved CASA model exhibited a high degree of correlation in both spatially dense and sparse vegetation areas (Figure 3c). These findings indicated that the lower accuracy of the CASA model resulting from the NDVI saturation problem can be addressed by utilizing EVI, which has been demonstrated to be more reliable in high vegetation coverage scenarios and is adapted to the response of soil, canopy background signal, and climate to vegetation [20]. It is, therefore, imperative that NDVI be replaced with EVI in the CASA model when operating in areas of high vegetation biomass. The model proposed in this study is of significant importance for the estimation of NPP through remote sensing in regions where extensive areas of sparse and dense vegetation coexist.

The improved CASA model has certain limitations, particularly in overestimating NPP in low-productivity areas (e.g., grasslands) and underestimating it in high-productivity areas (e.g., forests). This issue has been highlighted by other studies [79,80], suggesting that model accuracy could be enhanced in specific regions. Additionally, due to the challenge of directly measuring NPP, this study relies on the FLUXNET and ChinaFlux datasets to convert biomass data into NPP estimates. However, these derived NPP values may not fully represent actual NPP, as a single pixel may contain multiple vegetation types, while field observations typically focus on a single plant species [81,82]. As a result, remote sensing-based model outputs may not perfectly align with ground-based measurements. Another limitation is the lack of long-term, detailed field observations for validation, especially in forested areas, which narrows the validation scope and relies on MODIS products. Furthermore, using satellite data to estimate NPP may not capture the full complexity of local ecological processes, particularly in remote regions with limited observation points.

4.2. Effects of Urbanization and Climate Change on NPP Under Different HQ

In the context of global warming and socio-economic development, the impacts of urbanization and climate change on NPP have become increasingly significant [83]. Over the past few decades, global NPP has generally exhibited an upward trend; however, the driving factors have varied considerably across different periods and regions [84]. Climate change is closely linked to NPP changes through its effects on vegetation growth cycles and the hydrothermal conditions of ecosystems [85]. With the rapid urbanization in China in recent years, urbanization has emerged as a key factor influencing NPP [86]. While the effects of climate factors on NPP are well-studied and can be relatively easily quantified using models and remote sensing data, the complexity and variability of urbanization—driven by social, economic, and policy factors—make its impact on NPP much more challenging to quantify [87]. There is a close relationship between habitat quality (HQ) and NPP. Studies have shown that high HQ not only provides more suitable growth conditions for vegetation, enhancing photosynthetic efficiency but also increases NPP [88]. Furthermore, the ecological feedback mechanisms of vegetation can further optimize HQ, creating a positive feedback loop that strengthens ecosystem functions [31]. This study adopts a novel approach to explore the driving factors of NPP under different HQ conditions. By conducting scenario simulations, we have separated the effects of urbanization and climate change on NPP, effectively explaining the relative contributions of these factors under varying HQ conditions. This research provides theoretical support for future ecological management and policy development.

This study found that in low HQ areas, NPP tends to increase significantly, primarily due to the prevalence of vegetation types such as meadows, which benefit from adequate soil moisture and favorable light conditions [89,90]. In contrast, in areas with extremely high HQ, such as forested regions, NPP often decreases. This decline is attributed to human disturbances, such as logging and development activities, which disrupt the sensitive ecosystems in these areas [91]. These findings suggest that future ecological conservation efforts should prioritize resource management in high HQ regions to mitigate the negative impacts of human activities on NPP.

The impact of urbanization on NPP in the Qinghai–Tibet Plateau exhibits significant spatial heterogeneity. Overall, urbanization tends to have a negative effect on ecosystem productivity, particularly in regions with extremely high HQ. Urban expansion typically results in a reduction in NPP in urban centers, while NPP may increase in suburban areas, primarily due to low-density development and vegetation planting [92,93]. This contrasts with urbanization trends in other regions, where NPP generally decreases in urbanized areas. In urban centers, land use changes and high-density development are the primary drivers of reduced NPP. These findings highlight the importance of sustainable urban planning, especially in areas with high natural vegetation productivity, where urbanization may disrupt mature and sensitive ecosystems more vulnerable to land use changes [94,95]. In addition to urbanization, climate change (particularly temperature and precipitation) has been identified as a primary driver of NPP variation in this region. Numerous studies have confirmed that NPP increases with rising temperatures, especially in cooler areas where vegetation growth is more constrained [96,97]. This aligns with findings from the Qinghai–Tibet Plateau, where climate warming has been shown to enhance NPP, particularly in low HQ areas where vegetation is more sensitive to climate fluctuations [98,99]. Research indicates that temperature is the most significant climate factor affecting NPP, with 74.3% of vegetation benefiting from temperature increases. Precipitation plays a secondary role, particularly in arid and semi-arid regions with low to moderate HQ, where increased rainfall improves hydrothermal conditions, thereby supporting vegetation growth [100,101]. In extremely high HQ areas, such as the southeastern Qinghai–Tibet Plateau, monsoon rainfall provides ample water resources for vegetation. However, increased rainfall is often associated with reduced solar radiation, which can hinder photosynthesis and reduce productivity in some regions [102,103]. This interaction between water availability and light exposure complicates the relationship between climate factors and NPP. Vegetation in high HQ areas benefits from increased radiation, while shallow-

rooted grasses in low to moderate HQ areas thrive under reduced radiation, due to lower evaporation rates [104,105].

Overall, climate change is the primary driver of NPP variability in the Qinghai–Tibet Plateau, accounting for 69% of total NPP change. In contrast, the impact of urbanization on NPP is relatively small, contributing only 17% to overall NPP variation. This underscores the need for adaptive climate strategies to protect vegetation productivity in the region, particularly in low HQ areas, which are more vulnerable to climate fluctuations. Urbanization also warrants attention, especially regarding unsustainable practices such as logging and overgrazing, which contribute to ecological degradation. While urbanization poses challenges to NPP, the more substantial impact of climate change highlights the importance of focusing on climate adaptation measures to ensure ecosystem resilience in the face of ongoing environmental changes [106].

4.3. Research Limitations and Future Research Directions

This study used the mean value of HQ for partitioning; however, this approach has certain limitations. HQ exhibits dynamic spatial and temporal variation, and using mean values for partitioning overlooks the heterogeneity within local regions and its temporal fluctuations [107]. Such simplification may fail to fully capture NPP variation under different HQ conditions. Therefore, future research should adopt a dynamic approach to HQ, accounting for both spatial and temporal variability, to better analyze NPP drivers. Additionally, this study does not provide a detailed analysis of the specific factors influencing HQ. While changes in HQ are closely linked to climate factors and land use [108], the roles of these factors have not been fully examined. Future research should systematically assess the combined impacts of factors such as soil quality, vegetation type, and land management practices on HQ. This would contribute to a more comprehensive understanding of NPP variation and its drivers across different HQ levels. Furthermore, the role of social factors in urbanization is complex and multifaceted; yet, this paper does not fully address the social, economic, and policy-related aspects [109]. Urbanization involves not only spatial expansion but also various social dynamics, such as population growth, industrial structure, and policy regulation. The impact of these factors on NPP should be quantified in future studies [110]. Further research could explore the interaction between socioeconomic factors and urbanization, particularly in regions undergoing rapid policy and economic changes, to more comprehensively assess the long-term effects of urbanization on NPP.

5. Conclusions

The NPP product for the Tibetan Plateau was simulated at a resolution of 0.083° over the past two decades using an improved CASA model. A novel approach was then proposed to examine the mechanisms influencing NPP across various HQ regions through spatiotemporal analyses at both pixel and regional scales. From 2000 to 2020, NPP increased at a moderate rate of 0.28 g C m^{-2} per year ($p > 0.05$) in urban areas. This suggests that urban expansion did not lead to a reduction in plant biomass or the loss of productive land in expanding urban areas. In most regions, NPP was positively correlated with temperature and precipitation, while radiation exhibited a negative correlation. These factors collectively contributed to a modest increase in NPP across the Tibetan Plateau. The minimal NPP change associated with urbanization, combined with a significant increase in NPP due to climate change, resulted in an overall upward trend in NPP from 2000 to 2020. On the Tibetan Plateau, the average relative contributions of urbanization, climate change, and other factors to NPP change were 17%, 69%, and 14%, respectively. This approach offers significant potential for modeling the impact of urbanization on the carbon cycle, particularly in the context of the rapid changes driven by both urban expansion and climate change.

Supplementary Materials: The following supporting information can be downloaded at: https://www.mdpi.com/article/10.3390/land13122139/s1.

Author Contributions: T.X.: Methodology, Software, Formal analysis, Writing—original draft preparation. L.H.: Methodology, Software, Formal Analysis, Resources, Supervision. C.R.: Methodology, Data curation, Writing—review and editing. Q.X.: Investigation, Data curation, Visualization. D.Z.: Methodology, Investigation, Resources. G.S.: Software, Validation, Visualization. Z.F.: Conceptualization, Writing—review and editing, Supervision. All authors have read and agreed to the published version of the manuscript.

Funding: This research was supported by the Natural Science Foundation of Shandong Province, grant numbers ZR2020MD018 and ZR2020MD015; and by the National Natural Science Foundation of China, grant number 42171413.

Data Availability Statement: The original contributions presented in the study are included in the article; further inquiries can be directed to the corresponding author.

Acknowledgments: We would like to thank the kind help of the editor and the reviewers for improving the manuscript.

Conflicts of Interest: The authors declare no conflicts of interest.

References

1. Liu, Y.; Han, X.; Weng, F.; Xu, Y.; Zhang, Y.; Tang, S. Estimation of terrestrial net primary productivity in China from Fengyun-3D satellite data. *J. Meteorol. Res.* **2022**, *36*, 401–416. [CrossRef]
2. Park, J.H.; Gan, J.; Park, C. Discrepancies between global forest net primary productivity estimates derived from MODIS and forest inventory data and underlying factors. *Remote Sens.* **2021**, *13*, 1441. [CrossRef]
3. Hao, R.; Yu, D.; Huang, T.; Li, S.; Qiao, J. NPP plays a constraining role on water-related ecosystem services in an alpine ecosystem of Qinghai, China. *Ecol. Indic.* **2022**, *138*, 108846. [CrossRef]
4. Naeem, S.; Zhang, Y.; Tian, J.; Qamer, F.M.; Latif, A.; Paul, P.K. Quantifying the impacts of anthropogenic activities and climate variations on vegetation productivity changes in China from 1985 to 2015. *Remote Sens.* **2020**, *12*, 1113. [CrossRef]
5. Fokeng, R.M.; Fogwe, Z.N. Landsat NDVI-based vegetation degradation dynamics and its response to rainfall variability and anthropogenic stressors in Southern Bui Plateau, Cameroon. *Geosystems Geoenvironment* **2022**, *1*, 100075. [CrossRef]
6. Sun, H.; Chen, Y.; Xiong, J.; Ye, C.; Yong, Z.; Wang, Y.; He, D.; Xu, S. Relationships between climate change, phenology, edaphic factors, and net primary productivity across the Tibetan Plateau. *Int. J. Appl. Earth Obs. Geoinf.* **2022**, *107*, 102708. [CrossRef]
7. Boussema SB, F.; Allouche, F.K.; Ajmi, R.; Chaabane, B.; Gad, A.A. Assessing and monitoring the effects of land cover changes in biodiversity. Case study: Mediterranean coastal region, Sousse, Tunisia. *Egypt. J. Remote Sens. Space Sci.* **2023**, *26*, 185–196. [CrossRef]
8. Chen, Y.; Feng, X.; Tian, H.; Wu, X.; Gao, Z.; Feng, Y.; Piao, S.; Lv, N.; Pang, N.; Fu, B. Accelerated increase in vegetation carbon sequestration in China after 2010: A turning point resulting from climate and human interaction. *Glob. Chang. Biol.* **2021**, *27*, 5848–5864. [CrossRef]
9. Jha, S.; Srivastava, R. Impact of drought on vegetation carbon storage in arid and semi-arid regions. *Remote Sens. Appl. Soc. Environ.* **2018**, *11*, 22–29. [CrossRef]
10. Li, H.; Ding, J.; Zhang, J.; Yang, Z.; Yang, B.; Zhu, Q.; Peng, C. Effects of land cover changes on net primary productivity in the terrestrial ecosystems of China from 2001 to 2012. *Land* **2020**, *9*, 480. [CrossRef]
11. Hu, Q.; Li, T.; Deng, X.; Wu, T.; Zhai, P.; Huang, D.; Fan, X.; Zhu, Y.; Lin, Y.; Xiao, X.; et al. Intercomparison of global terrestrial carbon fluxes estimated by MODIS and Earth system models. *Sci. Total Environ.* **2022**, *810*, 152231. [CrossRef] [PubMed]
12. Chirici, G.; Chiesi, M.; Fibbi, L.; Giannetti, F.; Corona, P.; Maselli, F. High spatial resolution modelling of net forest carbon fluxes based on ground and remote sensing data. *Agric. For. Meteorol.* **2022**, *316*, 108866. [CrossRef]
13. Ma, F.; Jiang, Q.O.; Xu, L.; Lv, K.; Chang, G. Processes, potential, and duration of vegetation restoration under different modes in the eastern margin ecotone of Qinghai-Tibet Plateau. *Ecol. Indic.* **2021**, *132*, 108267. [CrossRef]
14. Zhang, J.; Hao, X.; Hao, H.; Fan, X.; Li, Y. Climate change decreased net ecosystem productivity in the arid region of central Asia. *Remote Sens.* **2021**, *13*, 4449. [CrossRef]
15. Gwal, S.; Singh, S.; Gupta, S.; Anand, S. Understanding forest biomass and net primary productivity in Himalayan ecosystem using geospatial approach. *Model. Earth Syst. Environ.* **2020**, *6*, 2517–2534. [CrossRef]
16. Guo, D.; Song, X.; Hu, R.; Zhu, X.; Jiang, Y.; Cai, S.; Zhang, Y.; Cui, X. Large-scale analysis of the spatiotemporal changes of Net Ecosystem Production in Hindu Kush Himalayan Region. *Remote Sens.* **2021**, *13*, 1180. [CrossRef]
17. Sun, J.; Yue, Y.; Niu, H. Evaluation of NPP using three models compared with MODIS-NPP data over China. *PLoS ONE* **2021**, *16*, e0252149.
18. Liu, Z.; Hu, M.; Hu, Y.; Wang, G. Estimation of net primary productivity of forests by modified CASA models and remotely sensed data. *Int. J. Remote Sens.* **2018**, *39*, 1092–1116. [CrossRef]

19. Benedetti, Y.; Callaghan, C.T.; Ulbrichová, I.; Galanaki, A.; Kominos, T.; Abou Zeid, F.; Ibáñez-Álamo, J.D.; Suhonen, J.; Díaz, M.; Bussière, R.; et al. EVI and NDVI as proxies for multifaceted avian diversity in urban areas. *Ecol. Appl.* **2023**, *33*, e2808. [CrossRef]
20. Liu, H.Q.; Huete, A. A feedback based modification of the NDVI to minimize canopy background and atmospheric noise. *IEEE Trans. Geosci. Remote Sens.* **1995**, *33*, 457–465. [CrossRef]
21. Li, H.; He, Y.; Zhang, L.; Cao, S.; Sun, Q. Spatiotemporal changes of Gross Primary Production in the Yellow River Basin of China under the influence of climate-driven and human-activity. *Glob. Ecol. Conserv.* **2023**, *46*, e02550. [CrossRef]
22. Guo, B.; Yang, F.; Fan, Y.; Zang, W. The dominant driving factors of rocky desertification and their variations in typical mountainous karst areas of Southwest China in the context of global change. *Catena* **2023**, *220*, 106674. [CrossRef]
23. Zhang, J.; Yuan, M.S.; Zhang, J.; Li, H.; Wang, J.; Zhang, X.; Ju, J.; Jiang, B.; Chen, H.; Zhu, Q. Responses of the NDVI of alpine grasslands on the Qinghai-Tibetan Plateau to climate change and human activities over the last 30 years. *Acta Ecol. Sin.* **2020**, *40*, 6269–6281.
24. Liu, Z.Y.; Zhang, J.; Chen, L. The latest change in the Qinghai-Tibetan Plateau vegetation index and its relationship with climate factors. *Clim. Environ. Res.* **2017**, *22*, 289.
25. Li, L.; Zhang, Y.; Wu, J.; Li, S.; Zhang, B.; Zu, J.; Zhang, H.; Ding, M.; Paudel, B. Increasing sensitivity of alpine grasslands to climate variability along an elevational gradient on the Qinghai-Tibet Plateau. *Sci. Total Environ.* **2019**, *678*, 21–29. [CrossRef]
26. Guo, B.; Lu, M.; Fan, Y.; Wu, H.; Yang, Y.; Wang, C. A novel remote sensing monitoring index of salinization based on three-dimensional feature space model and its application in the Yellow River Delta of China. *Geomat. Nat. Hazards Risk* **2023**, *14*, 95–116. [CrossRef]
27. Xiong, Q.; Xiao, Y.; Halmy, M.W.A.; Dakhil, M.A.; Liang, P.; Liu, C.; Zhang, L.; Pandey, B.; Pan, K.; Kafraway, S.B.E.; et al. Monitoring the impact of climate change and human activities on grassland vegetation dynamics in the northeastern Qinghai-Tibet Plateau of China during 2000–2015. *J. Arid Land* **2019**, *11*, 637–651. [CrossRef]
28. Wei, Y.Q.; Lu, H.Y.; Wang, J.N.; Sun, J.; Wang, X.F. Responses of vegetation zones, in the Qinghai-Tibetan Plateau, to climate change and anthropogenic influences over the last 35 years. *Pratacultural Sci.* **2019**, *36*, 1163–1176.
29. Yu, G.R.; Yang, M. Ecological economics foundation research on ecological values, ecological asset management, and value realization: Scientific concepts, basic theories, and realization paths. *J. Appl. Ecol.* **2022**, *33*, 1153–1165.
30. Aznarez, C.; Svenning, J.C.; Taveira, G.; Baró, F.; Pascual, U. Wildness and habitat quality drive spatial patterns of urban biodiversity. *Landsc. Urban. Plan.* **2022**, *228*, 104570. [CrossRef]
31. Mengist, W.; Soromessa, T.; Feyisa, G.L. Landscape change effects on habitat quality in a forest biosphere reserve: Implications for the conservation of native habitats. *J. Clean. Prod.* **2021**, *329*, 129778. [CrossRef]
32. Field, C.B.; Randerson, J.T.; Malmström, C.M. Global net primary production: Combining ecology and remote sensing. *Remote Sens. Environ.* **1995**, *51*, 74–88. [CrossRef]
33. Biggs, R.; Schlüter, M.; Biggs, D.; Bohensky, E.L.; BurnSilver, S.; Cundill, G.; Dakos, V.; Daw, T.M.; Evans L s Kotschy, K.; Leitch, A.M.; et al. Toward principles for enhancing the resilience of ecosystem services. *Annu. Rev. Environ. Resour.* **2012**, *37*, 421–448. [CrossRef]
34. Yang, J.; Xie, B.; Zhang, D. The trade-offs and synergistic relationships between grassland ecosystem functions in the yellow river basin. *Diversity* **2021**, *13*, 505. [CrossRef]
35. Peng, Q.; Wang, R.; Jiang, Y.; Li, C. Contributions of climate change and human activities to vegetation dynamics in Qilian Mountain National Park, northwest China. *Glob. Ecol. Conserv.* **2021**, *32*, e01947. [CrossRef]
36. Chen, T.; Tang, G.; Yuan, Y.; Guo, H.; Xu, Z.; Jiang, G.; Chen, X. Unraveling the relative impacts of climate change and human activities on grassland productivity in Central Asia over last three decades. *Sci. Total Environ.* **2020**, *743*, 140649. [CrossRef]
37. Wen, Y.; Liu, X.; Bai, Y.; Sun, Y.; Yang, J.; Lin, K.; Pei, F.; Yan, Y. Determining the impacts of climate change and urban expansion on terrestrial net primary production in China. *J. Environ. Manag.* **2019**, *240*, 75–83. [CrossRef]
38. Xin, Z.; Xu, J.; Zheng, W. Spatiotemporal variations of vegetation cover on the Chinese Loess Plateau (1981–2006): Impacts of climate changes and human activities. *Sci. China Ser. D Earth Sci.* **2008**, *51*, 67–78. [CrossRef]
39. Wen, Y.; Yang, J.; Liao, W.; Xiao, J.; Yan, S. Refined assessment of space-time changes, influencing factors and socio-economic impacts of the terrestrial ecosystem quality: A case study of the GBA. *J. Environ. Manag.* **2023**, *345*, 118869. [CrossRef]
40. Yu, Q.; Lu, H.; Yao, T.; Xue, Y.; Feng, W. Enhancing sustainability of vegetation ecosystems through ecological engineering: A case study in the Qinghai-Tibet Plateau. *J. Environ. Manag.* **2023**, *325*, 116576. [CrossRef]
41. Sun, J.; Ye, C.; Liu, M.; Wang, Y.; Chen, J.; Wang, S.; Liu, X.; Liu, G.; Xu, M.; Li, R.; et al. Response of net reduction rate in vegetation carbon uptake to climate change across a unique gradient zone on the Tibetan Plateau. *Environ. Res.* **2022**, *203*, 111894. [CrossRef] [PubMed]
42. Liu, H.; Fan, J.; Zhou, K.; Xu, X.; Zhang, H.; Guo, R.; Chen, S. Assessing the dynamics of human activity intensity and its natural and socioeconomic determinants in Qinghai–Tibet Plateau. *Geogr. Sustain.* **2023**, *4*, 294–304. [CrossRef]
43. Shi, F.; Liu, S.; An, Y.; Sun, Y.; Zhao, S.; Liu, Y.; Li, M. Climatic factors and human disturbance influence ungulate species distribution on the Qinghai-Tibet Plateau. *Sci. Total Environ.* **2023**, *869*, 161681. [CrossRef] [PubMed]
44. Liu, J.; Xin, Z.; Huang, Y.; Yu, J. Climate suitability assessment on the Qinghai-Tibet Plateau. *Sci. Total Environ.* **2022**, *816*, 151653. [CrossRef]
45. Geng, X.; Wang, X.; Fang, H.; Ye, J.; Han, L.; Gong, Y.; Cai, D. Vegetation coverage of desert ecosystems in the Qinghai-Tibet Plateau is underestimated. *Ecol. Indic.* **2022**, *137*, 108780. [CrossRef]

46. Zhu, H.; Su, D.; Yao, F. Spatio-Temporal Differences in Economic Security of the Prefecture-Level Cities in Qinghai–Tibet Plateau Region of China: Based on a Triple-Dimension Analytical Framework of Economic Geography. *Int. J. Environ. Res. Public Health* **2022**, *19*, 10605. [CrossRef]
47. Zhang, Y.; Yu, G.; Yang, J.; Wimberly, M.C.; Zhang, X.; Tao, J.; Jiang, Y.; Zhu, J. Climate-driven global changes in carbon use efficiency. *Glob. Ecol. Biogeogr.* **2014**, *23*, 144–155. [CrossRef]
48. Wang, X.; Tan, K.; Chen, B.; Du, P. Assessing the spatiotemporal variation and impact factors of net primary productivity in China. *Sci. Rep.* **2017**, *7*, 44415. [CrossRef]
49. Huang, C.; Sun, C.; Nguyen, M.; Wu, Q.; He, C.; Yang, H.; Tu, P.; Hong, S. Spatio-temporal dynamics of terrestrial Net ecosystem productivity in the ASEAN from 2001 to 2020 based on remote sensing and improved CASA model. *Ecol. Indic.* **2023**, *154*, 110920. [CrossRef]
50. Zhu, W.Q.; Pan, Y.Z.; Zhang, J.S. Estimation of net primary productivity of Chinese terrestrial vegetation based on remote sensing. *Chin. J. Plant Ecol.* **2007**, *31*, 413.
51. Zhu, W.; Pan, Y.; He, H.; Yu, D.; Hu, H. Simulation of maximum light use efficiency for some typical vegetation types in China. *Chin. Sci. Bull.* **2006**, *51*, 457–463. [CrossRef]
52. Zhou, N.; Hubacek, K.; Roberts, M. Analysis of spatial patterns of urban growth across South Asia using DMSP-OLS nighttime lights data. *Appl. Geogr.* **2015**, *63*, 292–303. [CrossRef]
53. Ma, T.; Zhou, Y.; Zhou, C.; Haynie, S.; Pei, T.; Xu, T. Night-time light derived estimation of spatio-temporal characteristics of urbanization dynamics using DMSP/OLS satellite data. *Remote Sens. Environ.* **2015**, *158*, 453–464. [CrossRef]
54. Lin, Y.P.; Lin, W.C.; Wang, Y.C.; Lien, W.Y.; Huang, T.; Hsu, C.C.; Schmeller, D.S.; Crossman, N.D. Systematically designating conservation areas for protecting habitat quality and multiple ecosystem services. *Environ. Model. Softw.* **2017**, *90*, 126–146. [CrossRef]
55. Wu, J.; Luo, J.; Zhang, H.; Qin, S.; Yu, M. Projections of land use change and habitat quality assessment by coupling climate change and development patterns. *Sci. Total Environ.* **2022**, *847*, 157491. [CrossRef]
56. Li, L.; Fan, Z.; Feng, W.; Yuxin, C.; Keyu, Q. Coupling coordination degree spatial analysis and driving factor between socio-economic and eco-environment in northern China. *Ecol. Indic.* **2022**, *135*, 108555. [CrossRef]
57. Zhang, Y.; Li, Y.; Wei, X.; Yang, Y.; Liu, L.; Murphey, Y.L. Graph matching for knowledge graph alignment using edge-coloring propagation. *Pattern Recognit.* **2023**, *144*, 109851. [CrossRef]
58. Feng, Y.; He, S.; Li, G. Interaction between urbanization and the eco-environment in the Pan-Third Pole region. *Sci. Total Environ.* **2021**, *789*, 148011. [CrossRef]
59. Naikoo, M.W.; Talukdar, S.; Ishtiaq, M.; Rahman, A. Modelling built-up land expansion probability using the integrated fuzzy logic and coupling coordination degree model. *J. Environ. Manag.* **2023**, *325*, 116441. [CrossRef]
60. Fan, W.; Wang, H.; Liu, Y.; Liu, H. Spatio-temporal variation of the coupling relationship between urbanization and air quality: A case study of Shandong Province. *J. Clean. Prod.* **2020**, *272*, 122812. [CrossRef]
61. Zhu, P.; Liu, G.; He, J. Spatio-temporal variation and impacting factors of NPP from 2001 to 2020 in Sanjiangyuan region, China: A deep neural network-based quantitative estimation approach. *Ecol. Inform.* **2023**, *78*, 102345. [CrossRef]
62. Wang, G.; Peng, W.; Zhang, L.; Zhang, J. Quantifying the impacts of natural and human factors on changes in NPP using an optimal parameters-based geographical detector. *Ecol. Indic.* **2023**, *155*, 111018. [CrossRef]
63. Mu, W.; Zhu, X.; Ma, W.; Han, Y.; Huang, H.; Huang, X. Impact assessment of urbanization on vegetation net primary productivity: A case study of the core development area in central plains urban agglomeration, China. *Environ. Res.* **2023**, *229*, 115995. [CrossRef]
64. Sharma, S.; Joshi, P.K.; Fürst, C. Unravelling net primary productivity dynamics under urbanization and climate change in the western Himalaya. *Ecol. Indic.* **2022**, *144*, 109508. [CrossRef]
65. Wu, S.; Zhou, S.; Chen, D.; Wei, Z.; Dai, L.; Li, X. Determining the contributions of urbanisation and climate change to NPP variations over the last decade in the Yangtze River Delta, China. *Sci. Total Environ.* **2014**, *472*, 397–406. [CrossRef] [PubMed]
66. Li, M.; Li, Q.; Xue, M. Spatio-Temporal Changes of Vegetation Net Primary Productivity and Its Driving Factors on the Ti-betan Plateau from 1979 to 2018. *Atmosphere* **2024**, *15*, 579. [CrossRef]
67. Ye, C.; Sun, J.; Liu, M.; Xiong, J.; Zong, N.; Hu, J.; Huang, Y.; Duan, X.; Tsunekawa, A. Concurrent and lagged effects of extreme drought induce net reduction in vegetation carbon uptake on Tibetan Plateau. *Remote Sens.* **2020**, *12*, 2347. [CrossRef]
68. Wang, W.; Yang, J.; Yang, G. Coordination characteristics and influencing mechanisms of habitat quality, ecological sensitivity and net primary production: A case study on Yangtze river economic belt in China. *Environ. Dev.* **2024**, *49*, 100969. [CrossRef]
69. Fang, C. How to promote the green development of urbanization in the Tibetan Plateau? *J. Geogr. Sci.* **2023**, *33*, 639–654. [CrossRef]
70. Tian, M.; Wei, J.; Liu, J. A comparative ethnic study on the urban integration of the migrant populations in the Qinghai-Tibet Plateau during the process of urbanization. *J. Urban. Aff.* **2023**, *22*, 1–18. [CrossRef]
71. Meng, M.; Fan, W.; Lu, J.; Dong, X.; Wei, H. Research on the influence of energy utilization and economic development on human well-being in Qinghai-Tibet Plateau. *Sustainability* **2020**, *13*, 196. [CrossRef]
72. Fu, S.; Zhang, X.; Kuang, W.; Guo, C. Characteristics of Changes in Urban Land Use and Efficiency Evaluation in the Qing-hai–Tibet Plateau from 1990 to 2020. *Land* **2022**, *11*, 757. [CrossRef]
73. Post, E.; Alley, R.B.; Christensen, T.R.; Macias-Fauria, M.; Forbes, B.C.; Gooseff, M.N.; Iler, A.; Kerby, J.T.; Laidre, K.L.; Mann, M.E.; et al. The polar regions in a 2 C warmer world. *Sci. Adv.* **2019**, *5*, eaaw9883. [CrossRef]

74. Wang, Z.; Wu, J.; Niu, B.; He, Y.; Zu, J.; Li, M.; Zhang, X. Vegetation expansion on the Tibetan Plateau and its relationship with climate change. *Remote Sens.* **2020**, *12*, 4150. [CrossRef]
75. Zhang, M.; Liu, X.; Nazieh, S.; Wang, X.; Nkrumah, T.; Hong, S. Spatiotemporal distribution of grassland NPP in Gansu province, China from 1982 to 2011 and its impact factors. *PLoS ONE* **2020**, *15*, e0242609. [CrossRef]
76. Augustine, J.A.; Capotondi, A. Forcing for multidecadal surface solar radiation trends over Northern Hemisphere continents. *J. Geophys. Res. Atmos.* **2022**, *127*, e2021JD036342. [CrossRef]
77. Yu, L.; Zhang, M.; Wang, L.; Qin, W.; Jiang, D.; Li, J. Variability of surface solar radiation under clear skies over Qing-hai-Tibet Plateau: Role of aerosols and water vapor. *Atmos. Environ.* **2022**, *287*, 119286. [CrossRef]
78. Liu, X.; Pei, F.; Wen, Y.; Li, X.; Wang, S.; Wu, C.; Wu, C.; Cai, Y.; Wu, J.; Chen, J.; et al. Global urban expansion offsets climate-driven increases in terrestrial net primary productivity. *Nat. Commun.* **2019**, *10*, 5558. [CrossRef]
79. Yang, F.; He, P.; Ding, H.; Shi, Y. A monthly high-resolution net primary productivity dataset (30 m) of Qinghai Plateau from 1987 to 2021. *IEEE J. Sel. Top. Appl. Earth Obs. Remote Sens.* **2023**, *16*, 8262–8273. [CrossRef]
80. Pang, Y.; Chen, C.; Guo, B.; Qi, D.; Luo, Y. Impacts of Climate Change and Anthropogenic Activities on the Net Primary Productivity of Grassland in the Southeast Tibetan Plateau. *Atmosphere* **2023**, *14*, 1217. [CrossRef]
81. Zhang, Y.; Song, C.; Zhang, K.; Cheng, X.; Band, L.E.; Zhang, Q. Effects of land use/land cover and climate changes on terrestrial net primary productivity in the Yangtze River Basin, China, from 2001 to 2010. *J. Geophys. Res. Biogeosciences* **2014**, *119*, 1092–1109. [CrossRef]
82. Meraj, G.; Kanga, S.; Ambadkar, A.; Kumar, P.; Singh, S.K.; Farooq, M.; Johnson, B.A.; Rai, A.; Sahu, N. Assessing the yield of wheat using satellite remote sensing-based machine learning algorithms and simulation modeling. *Remote Sens.* **2022**, *14*, 3005. [CrossRef]
83. Qin, Z.; Sha, Z. Modeling the impact of urbanization and climate changes on terrestrial vegetation productivity in China by a neighborhood substitution analysis. *Ecol. Model.* **2023**, *482*, 110405. [CrossRef]
84. Wei, X.; Yang, J.; Luo, P.; Lin, L.; Lin, K.; Guan, J. Assessment of the variation and influencing factors of vegetation NPP and carbon sink capacity under different natural conditions. *Ecol. Indic.* **2022**, *138*, 108834. [CrossRef]
85. Gang, C.; Zhang, Y.; Wang, Z.; Chen, Y.; Yang, Y.; Li, J.; Cheng, J.; Qi, J.; Odeh, I. Modeling the dynamics of distribution, extent, and NPP of global terrestrial ecosystems in response to future climate change. *Glob. Planet. Chang.* **2017**, *148*, 153–165. [CrossRef]
86. Guan, X.; Shen, H.; Li, X.; Gan, W.; Zhang, L. A long-term and comprehensive assessment of the urbanization-induced impacts on vegetation net primary productivity. *Sci. Total Environ.* **2019**, *669*, 342–352. [CrossRef]
87. Fu, Y.; Lu, X.; Zhao, Y.; Zeng, X.; Xia, L. Assessment impacts of weather and land use/land cover (LULC) change on urban vegetation net primary productivity (NPP): A case study in Guangzhou, China. *Remote Sens.* **2013**, *5*, 4125–4144. [CrossRef]
88. Zhong, J.; Liu, J.; Jiao, L.; Lian, X.; Xu, Z.; Zhou, Z. Assessing the comprehensive impacts of different urbanization process on vegetation net primary productivity in Wuhan, China, from 1990 to 2020. *Sustain. Cities Soc.* **2021**, *75*, 103295. [CrossRef]
89. Geng, Y.; Wang, Y.; Yang, K.; Wang, S.; Zeng, H.; Baumann, F.; Kuehn, P.; Scholten, T.; He, J.S. Soil respiration in Tibetan alpine grasslands: Belowground biomass and soil moisture, but not soil temperature, best explain the large-scale patterns. *PLoS ONE* **2012**, *7*, e34968. [CrossRef]
90. Li, C.; Sun, H.; Liu, L.; Dou, T.; Zhou, M.; Li, W.; Wu, X. The importance of permafrost in the steady and fast increase in net primary production of the grassland on the Qinghai–Tibet Plateau. *Catena* **2022**, *211*, 105964. [CrossRef]
91. Luo, Z.; Wu, W.; Yu, X.; Song, Q.; Yang, J.; Wu, J.; Zhang, H. Variation of net primary production and its correlation with climate change and anthropogenic activities over the Tibetan Plateau. *Remote Sens.* **2018**, *10*, 1352. [CrossRef]
92. Peng, J.; Shen, H.; Wu, W.; Liu, Y.; Wang, Y. Net primary productivity (NPP) dynamics and associated urbanization driving forces in metropolitan areas: A case study in Beijing City, China. *Landsc. Ecol.* **2016**, *31*, 1077–1092. [CrossRef]
93. Gao, J.; Liu, M.; Wang, X. Unveiling the Impact of Urbanization on Net Primary Productivity: Insights from the Yangtze River Delta Urban Agglomeration. *Land.* **2024**, *13*, 562. [CrossRef]
94. Seto, K.C.; Güneralp, B.; Hutyra, L.R. Global forecasts of urban expansion to 2030 and direct impacts on biodiversity and carbon pools. *Proc. Natl. Acad. Sci. USA* **2012**, *109*, 16083–16088. [CrossRef]
95. Zhou, J.; Lu, T. Relative contributions of climate change and human activities on vegetation productivity variation in na-tional nature reserves on the Qinghai–Tibetan Plateau. *Remote Sens.* **2022**, *14*, 4626. [CrossRef]
96. Hu, L.; Fan, W.; Yuan, W.; Ren, H.; Cui, Y. Spatiotemporal variation of vegetation productivity and its feedback to climate change in Northeast China over the last 30 years. *Remote Sens.* **2021**, *13*, 951. [CrossRef]
97. Klemm, T.; Briske, D.D.; Reeves, M.C. Potential natural vegetation and NPP responses to future climates in the US Great Plains. *Ecosphere* **2020**, *11*, e03264. [CrossRef]
98. Azhdari, Z.; Rafeie Sardooi, E.; Bazrafshan, O.; Zamani, H.; Singh, V.P.; Mohseni Saravi, M.; Ramezani, M. Impact of climate change on net primary production (NPP) in south Iran. *Environ. Monit. Assess.* **2020**, *192*, 409. [CrossRef] [PubMed]
99. Cui, J.; Wang, Y.; Zhou, T.; Jiang, L.; Qi, Q. Temperature mediates the dynamic of MODIS NPP in alpine grassland on the Tibetan Plateau, 2001–2019. *Remote Sens.* **2022**, *14*, 2401. [CrossRef]
100. Stampfli, A.; Bloor, J.M.; Fischer, M.; Zeiter, M. High land-use intensity exacerbates shifts in grassland vegetation composi-tion after severe experimental drought. *Glob. Chang. Biol.* **2018**, *24*, 2021–2034. [CrossRef]

101. Stuart-Haëntjens, E.; De Boeck, H.J.; Lemoine, N.P.; Mänd, P.; Kröel-Dulay, G.; Schmidt, I.K.; Jentsch, A.; Stampfli, A.; An-deregg WR, L.; Bahn, M.; et al. Mean annual precipitation predicts primary production resistance and resilience to extreme drought. *Sci. Total Environ.* **2018**, *636*, 360–366. [CrossRef] [PubMed]
102. Du, R.; Wu, J.; Tian, F.; Yang, J.; Han, X.; Chen, M.; Zhao, B.; Lin, J. Reversal of soil moisture constraint on vegetation growth in North China. *Sci. Total Environ.* **2023**, *865*, 161246. [CrossRef]
103. Chen, A.; Huang, L.; Liu, Q.; Piao, S. Optimal temperature of vegetation productivity and its linkage with climate and ele-vation on the Tibetan Plateau. *Glob. Chang. Biol.* **2021**, *27*, 1942–1951. [CrossRef] [PubMed]
104. Blal, M.; Khelifi, S.; Dabou, R.; Sahouane, N.; Slimani, A.; Rouabhia, A.; Ziane, A.; Neçaibia, A.; Bouraiou, A.; Tidjar, B. A prediction models for estimating global solar radiation and evaluation meteorological effect on solar radiation potential under several weather conditions at the surface of Adrar environment. *Measurement* **2020**, *152*, 107348. [CrossRef]
105. Liao, Y.; Cao, H.X.; Liu, X.; Li, H.T.; Hu, Q.Y.; Xue, W.K. By increasing infiltration and reducing evaporation, mulching can improve the soil water environment and apple yield of orchards in semiarid areas. *Agric. Water Manag.* **2021**, *253*, 106936. [CrossRef]
106. Gang, C.; Zhou, W.; Li, J.; Chen, Y.; Mu, S.; Ren, J.; Chen, J.; Groisman, P.Y. Assessing the spatiotemporal variation in distribution, extent and NPP of terrestrial ecosystems in response to climate change from 1911 to 2000. *PLoS ONE* **2013**, *8*, e80394. [CrossRef] [PubMed]
107. Beerens, J.M.; Frederick, P.C.; Noonburg, E.G.; Gawlik, D.E. Determining habitat quality for species that demonstrate dynamic habitat selection. *Ecol. Evol.* **2015**, *5*, 5685–5697. [CrossRef]
108. Fan, X.; Gu, X.; Yu, H.; Long, A.; Tiando, D.S.; Ou, S.; Li, J.; Rong, Y.; Tang, G.; Zheng, Y.; et al. The spatial and temporal evolution and drivers of habitat quality in the Hung River Valley. *Land.* **2021**, *10*, 1369. [CrossRef]
109. Zhang, H.; Chen, M.; Liang, C. Urbanization of county in China: Spatial patterns and influencing factors. *J. Geogr. Sci.* **2022**, *32*, 1241–1260. [CrossRef]
110. Liu, Y.; Xu, M.; Guo, B.; Yang, G.; Li, J.; Yu, Y. Changes in the Vegetation NPP of Mainland China under the Combined Actions of Climatic-Socioeconomic Factors. *Forests* **2023**, *14*, 2341. [CrossRef]

Disclaimer/Publisher's Note: The statements, opinions and data contained in all publications are solely those of the individual author(s) and contributor(s) and not of MDPI and/or the editor(s). MDPI and/or the editor(s) disclaim responsibility for any injury to people or property resulting from any ideas, methods, instructions or products referred to in the content.